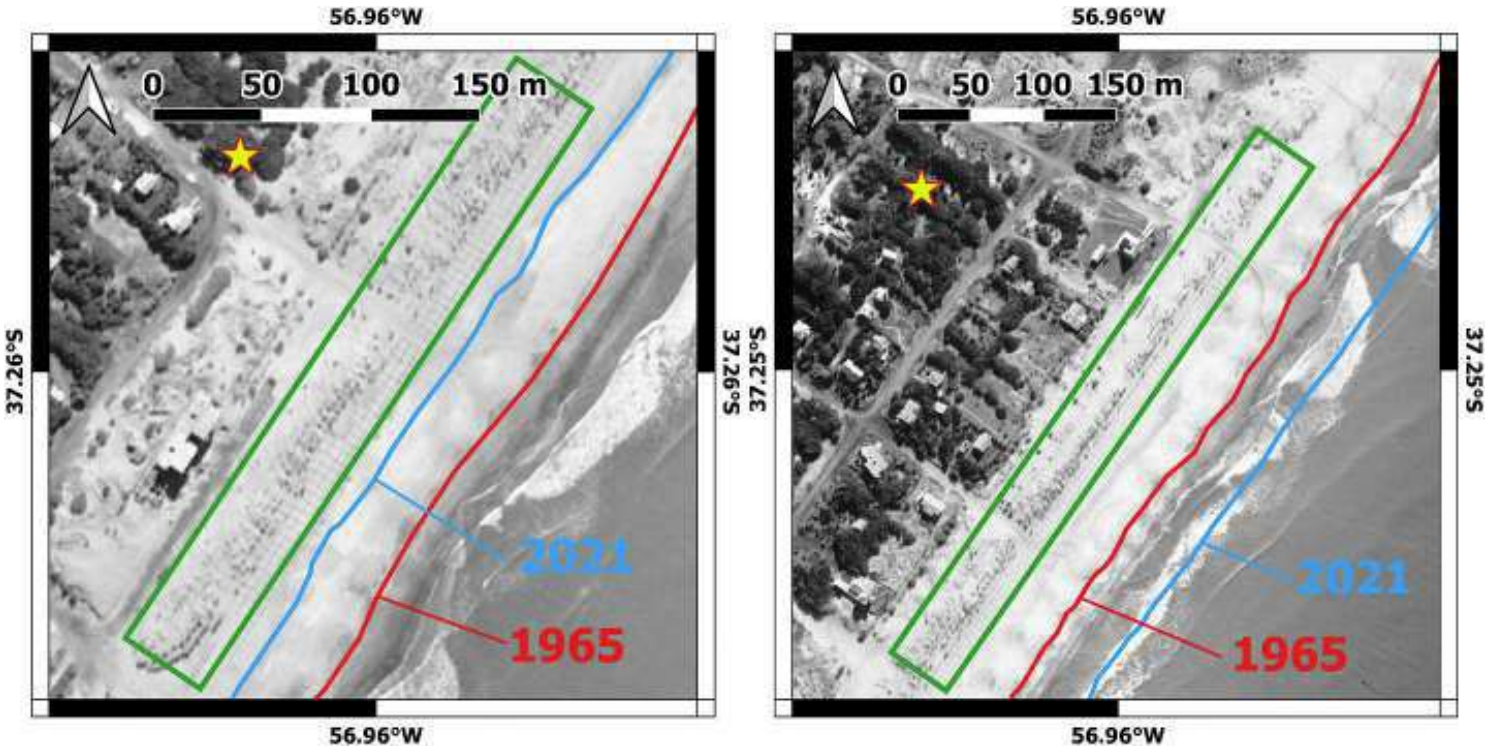
56.96°W
0 50 100 150 m
37.26°S
37.25°S
2021
1965
56.96°W
56.96°W
0 50 100 150 m
37.25°S
2021
1965
56.96°W

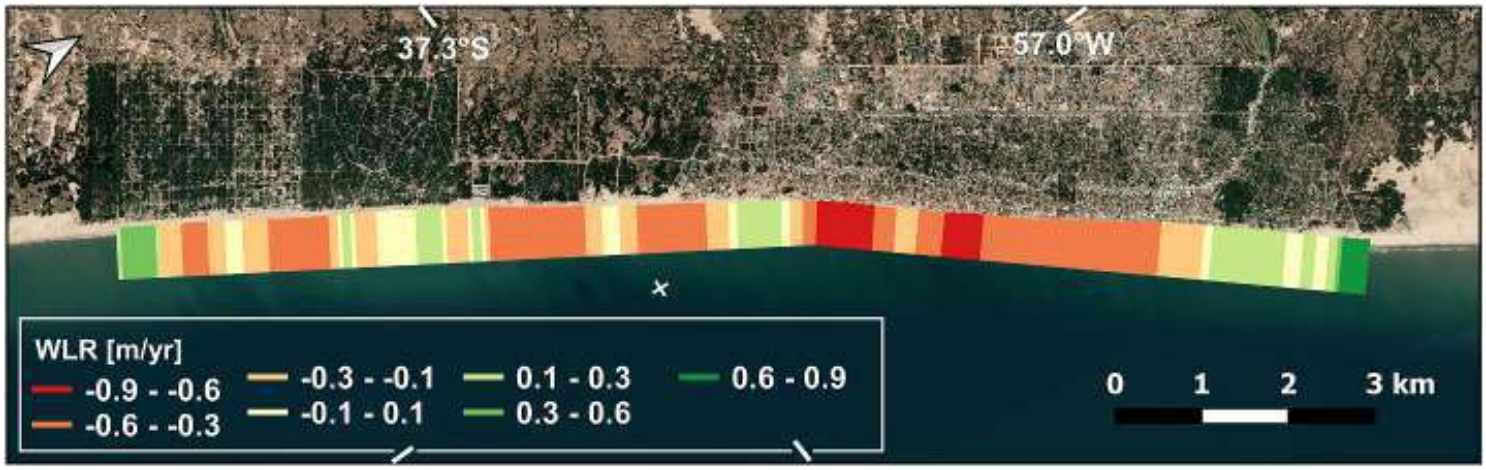
37.3°S
57.0°W
WLR [m/yr]
-0.9 - -0.6
-0.6 - -0.3
-0.3 - -0.1
-0.1 - 0.1
0.1 - 0.3
0.3 - 0.6
0.6 - 0.9
0 1 2 3 km

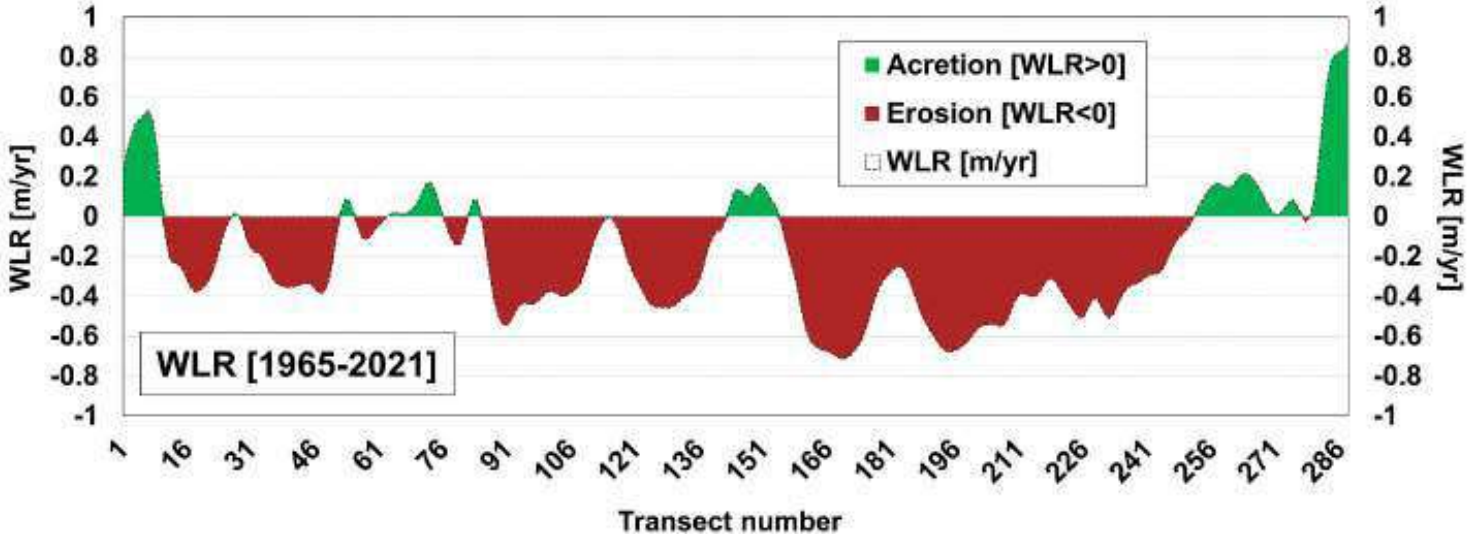
Acretion [WLR>0]
Erosion [WLR<0]
WLR [m/yr]
WLR [1965-2021]
WLR [m/yr]
Transect number

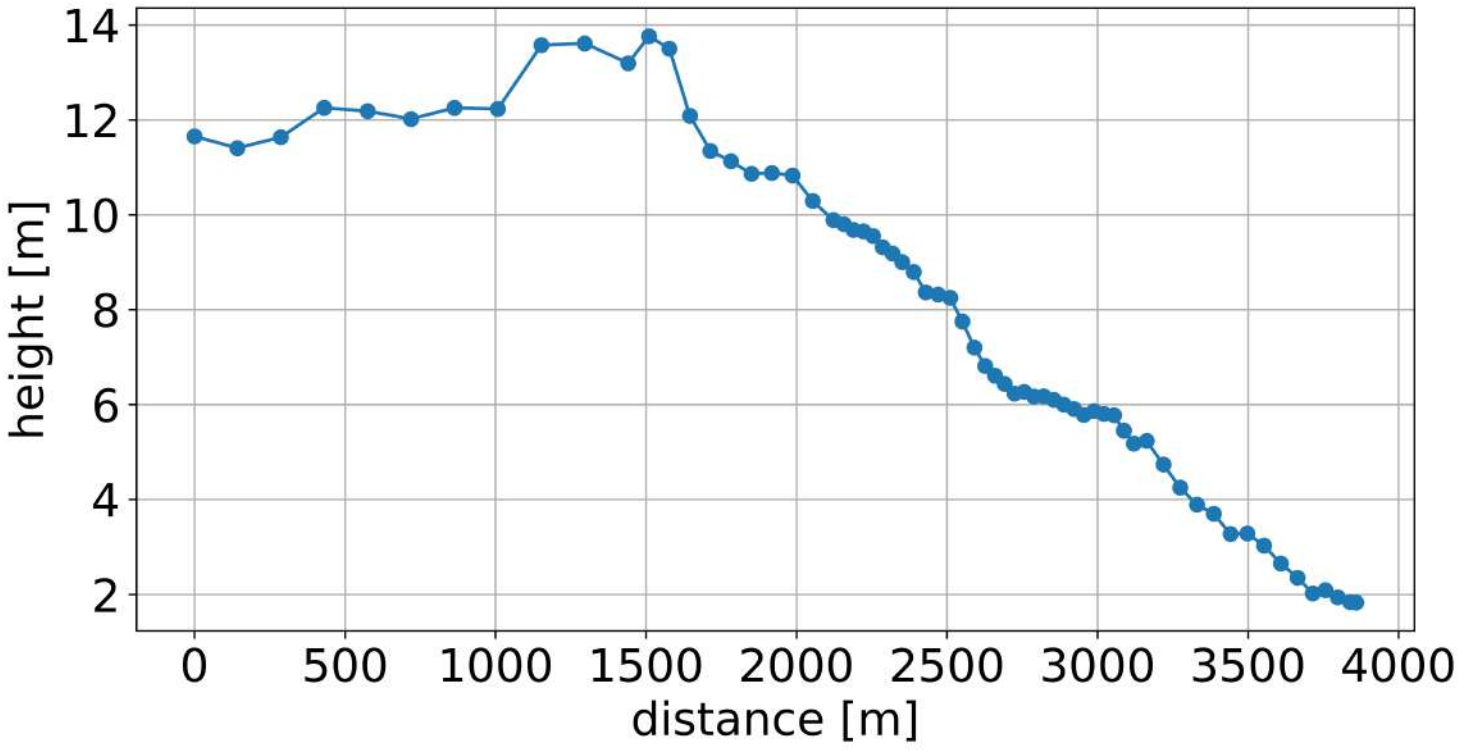
14
12
10
8
6
4
2
height [m]
0
500
1000
1500
2000
2500
3000
3500
4000
distance [m]

Journal of South American Earth Sciences 128 (2023) 104453

Contents lists available at ScienceDirect

Journal of South American Earth Sciences

journal homepage: www.elsevier.com/locate/jsames

Coastal erosion in temperate barriers: an anthropized sandy beach in Buenos Aires, Argentina

Pedro Andrés Garzo [a,b,*], Leonardo Sánchez-Caro [c], Marcia Mojica [a,b]

[a] Instituto de Geología de Costas y del Cuaternario (IGCC - UNMDP/CIC), Funes 3350, (7600), Mar Del Plata, Buenos Aires, Argentina
[b] Instituto de Investigaciones Marinas y Costeras (IIMyC - CONICET/UNMDP), Av. Juan B, Justo 2250, (7600), Mar Del Plata, Buenos Aires, Argentina
[c] Centro de Estudios Integrales de la Dinámica Exágena (CEIDE - UNLP/CONICET), Calle 64 N° 3, (1900), La Plata, Buenos Aires, Argentina

ARTICLE INFO

Keywords:
Digital Shoreline Analysis System
erosional hotspots
forecasting
shoreline change

ABSTRACT

Coastal erosion is a common issue in urbanized areas located on sandy barriers in Latin America, making them highly vulnerable to both natural and human induced disasters. This pose a significant threat to the long-term sustainability of these coastal systems. The main objective of this study was to evaluate the medium-term shoreline evolution of a highly-anthropized beach sector located within a coastal barrier system of Buenos Aires, Argentina. For this purpose, a geospatial analysis based on aerial imagery and high-resolution satellite data was conducted for the 1965–2021 period. Additionally, the study aimed to identify critical erosive sectors and to provide estimations for the near-future shoreline evolution of these beaches. The results showed contrasting patterns, with sectors presenting shoreline retreat rates up to 0.7 m/yr while others demonstrated accretion rates exceeding 0.6 m/yr. Despite these along-shore variations in erosion/accretion balances, more than 70% of the shoreline presented an erosional trend for the studied period. This led to the identification of an erosional hot spot covering 30% of the urbanized waterfront. Furthermore, the 2030 forecast suggests that a highly urbanized beach sector could suffer a shoreline retreat of about 20 m. These results could be directly linked to the historical land use/land cover changes, mainly related to dune stabilization processes and to the implantation of urban surfaces. At this point, erosive patterns could be mainly caused by local cross-shore imbalances due to these anthropogenic disturbances. It is expected that the results of the present study will serve as a basis for coastal management policies, and the proposed method will be a useful tool for assessing coastal erosion hazard.

1. Introduction

Coastal areas are highly important environments for socio-economic development and human well-being (Gogoberidze, 2012). Multiple uses and opportunities are linked to these areas due to their valuable ecosystem goods and services (Enriquez-Acevedo et al., 2018). Nowadays more than 40% of the Earth's population lives at less than 100 km away from the coast and about 10% lives in coastal zones below 10-m topographic altitude (Busayo and Kalumba, 2021). Moreover, population density is expected to increase about 25% for 2050 (Zhao et al., 2022).

However, their population concentration and the large number of economic activities involved, make them highly vulnerable to both natural and human induced disasters, as well as the impacts of climate change. These events pose significant threats to the long-term sustainability of coastal areas (Hanson et al., 2011; Neumann et al., 2015). Flooding, coastal erosion, saline intrusion and land subsidence (Pivel et al., 2001; Esteves et al., 2002; Dillenburg et al., 2004; Poulter and Halpin, 2008; Van Rijn, 2011; Rahman and Bhattacharya, 2014; Erkens et al., 2016; Barboza et al., 2018), among other impacts, affect coastal areas at a global scale.

Particularly, coastal erosion is a hazard that severely affects urbanized areas developed over barrier sectors (De Oliveira et al., 2019; Simões et al., 2022). Beaches are vital in tourism-based coastal economies (Phillips and Jones, 2006). The shoreline retreat causes diverse socioeconomic impacts including destruction of coastal infrastructure, landscape damage, loss of recreational value of beaches and economic impacts for the touristic sector (Esteves, 2004; Mentaschi et al., 2018).

Abbreviations: DSAS, Digital Shoreline Analysis System; EHS, Erosional Hotspot; EPR, End Point Rate; LULC, Land Use/Land Cover; MET, Maximum Erosional Transect; MAT, Maximum Accretional Transect; NSM, Net Shoreline Movement; SCE, Shoreline Change Envelope; WLR, Weighted Linear Regression.

* Corresponding author. Instituto de Geología de Costas y del Cuaternario (IGCC - UNMDP/CIC), Funes 3350, (7600), Mar Del Plata, Buenos Aires, Argentina.
E-mail address: pgarzo@agro.uba.ar (P.A. Garzo).

https://doi.org/10.1016/j.jsames.2023.104453
Received 30 December 2022; Received in revised form 9 June 2023; Accepted 13 June 2023
Available online 15 June 2023

Land use and land cover (LULC) changes are one of the main anthropogenic impacts over coastal areas around the world (Clark, 1997). El-Khalidi et al., 2021 identified the alternation of accretional and erosional sectors in the Mediterranean coast of Morocco in relation to LULC such as afforestation for dune fixation and coastal urbanization. Rangel-Buitrago et al. (2015) assessed erosional zones in the Colombian Caribe induced by coastal urbanization and mangrove destruction. By contrast, Ferreira et al. (2021) identified a highly stable coastline over the Parnaíba Delta, Brazil, attributable to a low anthropogenic influence over this area. In addition, some authors propose the restriction of LULC changes over those areas severely affected by coastal erosion processes (Coca and Ricaurte-Villota, 2022).

Remote sensing data has been widely used for monitoring changes in the Earth's surface (Coppin et al., 2002; Lu et al., 2004; Hansen and Loveland, 2012), including coastal areas (Cabezas-Rabadán et al., 2019; Garzo et al., 2019; Vos et al., 2019; Spinosa et al., 2021). Coastal erosion studies play a crucial role in supporting coastal management policies. Various methods based on imagery data have been developed to assess shoreline changes at different time scales (Scarelli et al., 2016, 2017; Gracia et al., 2018; Williams et al., 2018; Bilmes et al., 2019; Sowmya et al., 2019).

Thus, the spatial alternation of erosional and accretional sectors for continuous coastlines was documented by several authors (Domínguez et al., 2005; Anfuso et al., 2007; Virdis et al., 2012; Jana et al., 2016; Carvalho et al., 2020; Guimaraes-Santos et al., 2021; Zanchi-Watanabe et al., 2023; among others). Temporal changes in the erosional/accretional rates were also studied (Stive et al., 2002; Fletcher et al., 2003; Różyński, 2005; Pianca et al., 2015; Turner et al., 2016; Bitencourt et al., 2020; Dillenburg et al., 2020; Vallarino-Castillo et al., 2022, among others). In addition, this techniques enable the identification of erosional hotspots (EHS), defined by Kraus and Galgano (2001) as an area that erodes more rapidly than the adjacent beaches or than anticipated during design, and can be quantified and qualified by several metrics (e.g. loss of beach width, loss of sediment volume, or percentage of fill remaining of the amount placed).

Virdis et al. (2012) identified zones with accretional conditions as well as zones with highly erosional conditions alongshore in an 18 km study area in Sardinia, Italy, for the 1955–2010 period; Domínguez et al. (2005) documented shoreline change rates which ranged from strongly erosional to strongly accretional over a 23 km shoreline in south-western Spain between 1956 and 2021; Guimaraes-Santos et al. (2021) identified alternating accretional and erosional zones over a 17.6 km long coastal stretch in João Pessoa City, Brazil, for the 1985–2019 period; Vallarino-Castillo et al. (2022) observed different periods of erosional and accretional tendencies over 11.8 km of quaternary beaches in the Pacific Coast of Panamá between 1998 and 2021. In all those cases, the temporal and spatial alternation of erosional and accretional coastline sectors could be explained by geomorphological differences as well as coastal anthropization impacts (e.g. LULC changes, coastal tourism, defense structures or harbor development).

The Digital Shoreline Analysis System (DSAS) is an open source software application that works within the framework of the Esri Geographic Information System (ArcGIS) software. It is a widely used tool for computing rate-of-change statistics for a time series of shoreline vector data (Himmelstoss et al., 2018). It can be applied to a wide range of coastal settings and environments (Albuquerque et al., 2013; Rangel-Buitrago et al., 2015; Abreu et al., 2016; Martín Prieto et al., 2018; Nassar et al., 2018; Santos and Bonetti, 2018; Lemos and Sopchaki, 2020; Mishra et al., 2020; Villate-Daza et al., 2020; Martínez et al., 2022). This tool has been applied recently in Argentina (Cellone et al., 2016; D'Amico et al., 2019; Bacino et al., 2020), but only related to the fluvial or mixed coasts of the De La Plata River estuary.

The main objective of this work was to assess medium-term shoreline changes over a beach sector located in a coastal barrier system of Buenos Aires, Argentina. For this purpose, a geospatial analysis was carried out. Aerial imagery and high resolution remote sensing data for the 1965–2021 period was used; the DSAS software was implemented, being one of the first use cases of this technique in maritime coasts of Argentina; and GIS based techniques allowed the data and results interpretation. The study area constitutes a highly anthropized coast with an almost exclusively tourism-based economy and a background of several LULC changes since the '30s. At this point it was intended to identify erosional hot spots and accretional sectors as well as to propose a zonification related to historical shoreline evolution trends. Finally this study aimed to provide estimates for the near future evolution of these beaches. It is expected that the results of the present study will serve as a basis for coastal management policies, and the proposed method will be a useful tool for assessing coastal erosion hazard.

1.1. Eastern sandy barrier and study area

The coastal sandy barriers of Buenos Aires, Argentina, evolved in relation to the Mid-Holocene sea-level fluctuation as well as the great majority of barriers and spits of the South American coast (Isla, 1998; Isla and Angulo, 2016). This fluctuation affected the low-lying areas of the extensive plain of the Salado River basin, in the northeastern of the Buenos Aires Province, by burying coastal lagoons and marshes with a dune field (Isla et al., 1996). This process involved the formation of the Eastern Barrier, located in the northernmost sector of the Argentinian Atlantic Coast (Fig. 1).

According to previous studies (Schnack et al., 1982; Violante, 1992), this barrier grew from a former cape located approximately in the present day Villa Gesell City following a NNE-SSO direction. This evidence proposes a coastal drift reversal, taking into account that the undergoing beach drift is from south to north (Fasano et al., 1982). Transverse, parabolic, barchanoid and star dunes have been recognized in this barrier. They are mainly composed of mid-grain sands with the presence of fine textures in the inter-dune depressions (Isla et al., 1998). Changes in dune morphology was associated to natural colonization by psammophilous plants (*Panicum racemosum, Hydrocotyle bonariensis*, *Cakile maritima*, *Calycera crassifolia*, among other native species) that induced a reduction in the sand availability (Marcomini et al., 2017).

The exponential development shown by the "sun and beach" tourism during the second half of the XX century led to different LULC changes over this barrier. On the one hand, the afforestation processes for ground stabilization transformed active dunes into semi-fixed or fixed dune fields (Turno-Orellano and Isla, 2004). This process led to higher dunes but with narrower beaches. On the other hand, the impervious urban covers were established in replacement of natural sandy substrate. This provoked several changes in the hydrological local balance, including increases in surface runoff and diminish of coastal aquifer recharge areas (Carretero et al., 2014).

The study area of this work is delimited by the urban and peri-urban beaches of the Villa Gesell County, located in the Eastern Barrier of the Buenos Aires Province, Argentina. This county is represented by a total waterfront extent of approximately 60 km. However, the urbanized sector only comprises 14 km and it is divided into 4 coastal villages: Mar Azul, Las Gaviotas, Mar de Las Pampas and Villa Gesell (Fig. 1). Its beaches are represented by a micromareal and semi-diurnal tidal regime with a mean tidal amplitude of 0.74 m (SHN, Servicio de Hidrografía Naval de la República Argentina, 2021). These beaches are naturally dissipative. However, some sectors had turned into reflective beaches in response to anthropogenic impacts (Bértola, 2006). The littoral drift provides a continuous sand supply of about 400,000 m^3/yr in a S–N direction (Verón and Bértola, 2014). The mean wave height was recorded as 0.89 m and the peak wave period between 7 and 10 s for the neighboring county of Pinamar. Winds do not have a dominant direction as those from the south and north are abundant. However, southerly winds are the most intense and represent the extreme climate events (called sudestadas) (Lanfredi et al., 1992).

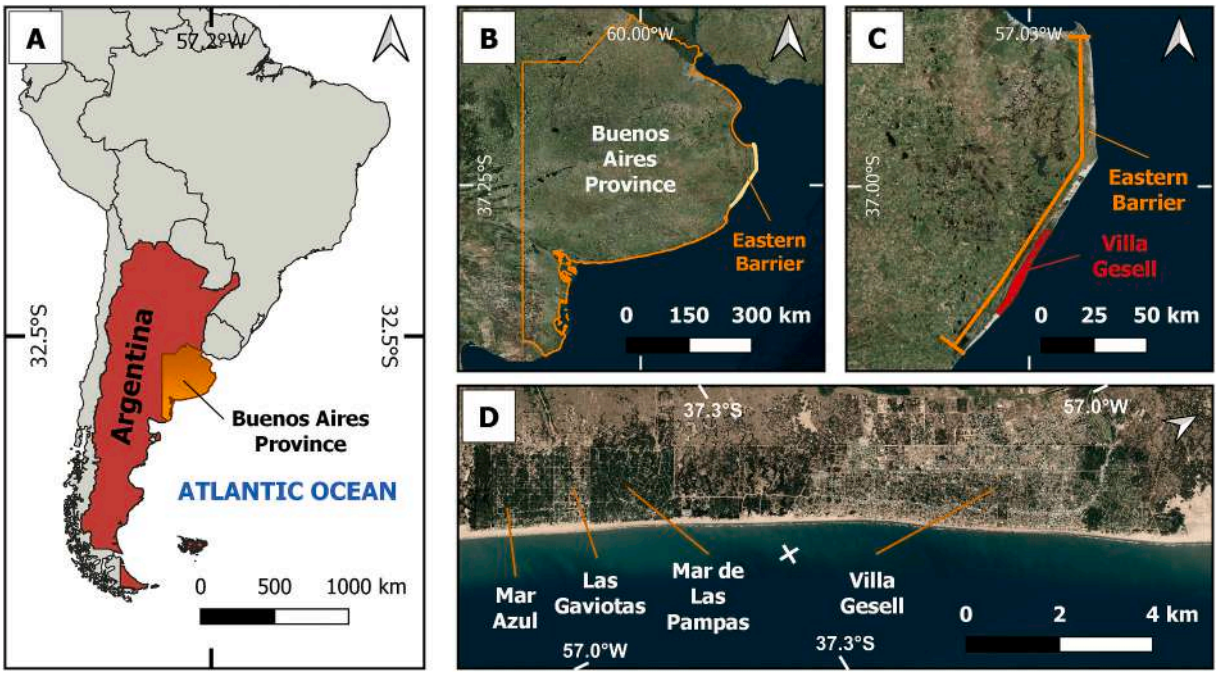

Fig. 1. Location of the Eastern Barrier in the Buenos Aires Province (B), Argentina (A). The Villa Gesell County's waterfront represents a total extension of about 60 km (C); this study only comprises the urbanized waterfront of about 14 km (D). Background image corresponds to the Google Satellite QuickMapService basemap for ArcGIS software.

2. Materials and methods

2.1. Method workflow

In order to assess the medium-term shoreline evolution in the study area, five main steps were conducted: imagery data acquisition and pre-proccesing, multitemporal shoreline position mapping, wave climate characterization, shoreline positional uncertainty estimation and shoreline change assessment. Fig. 2 schematically summarizes these steps, which are described in the following sections.

2.2. Imagery data

Five sets of aerial photographs were used to identify the shoreline position between 1965 and 1997 (Table 1). This dataset was retrieved from the National Geographic Institute (Instituto Geográfico Nacional - IGN), the Naval Hidropography Service (Servicio de Hidrografía Naval - SHN) and the Photogrammetry Division of the Ministry of Public Work (Ministerio de Obras Públicas - MOP). Images corresponding to 1965 and 1985 were firstly digitized by scanning at a 1200 dpi (dots per inch) resolution. The remaining (1975 and 1997) were already digitized. Pixel size of about 1 m or below is suggested for aerial orthophotos utilization (Araujo et al., 2009). The digitalization resolution was used in order to define pixel size of the images according to:

$$\text{Pixel size} = \frac{0.0254 \text{ x Spatial Scale [m]}}{\text{Resolution [dpi]}} \quad , \tag{1}$$

where the spatial scale was determined by the photogrammetric flight characteristics and the digitalization resolution depends on the quality of the scanning process.

In addition, two sets of satellite images corresponding to the QuickBird orbital sensor and available in the free access software GoogleEarth™ (GE; https://earth.google.com/web/) were retrieved for the years 2011 and 2021 (Table 2). Since this global representation imagery does not have a defined nominal scale, downloads were performed at a maximum resolution of 4800 × 2700 pixels and covering an area of

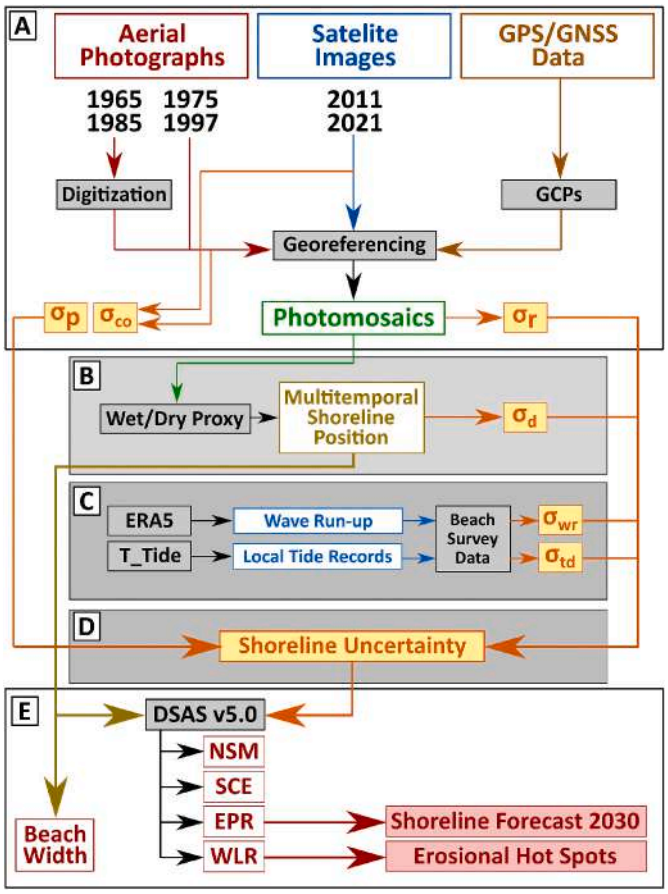

Fig. 2. Schematic workflow considering the main steps of this work: imagery data acquisition and pre-processing [A]; multitemporal shoreline mapping [B]; wave climate characterization [C]; shoreline positional uncertainty estimation [D]; and shoreline change assessment [E].

Table 1
Details of the aerial photographs. Source of the data, date, film type (B&W = Black and White), number of images used to make up the photomosaics; images' size and nominal scale; scanning resolution, pixel size, lineal waterfront coverage of each generated photomosaic and estimated RMSE.

Aerial Photograph	1965	1975	1985	1997
Source	SHN	MOP	MOP	MOP
Date	26 Jun 1965	14 Aug 1975	3 Dec 1985	6 Dec 1997
Film	B&W	B&W	B&W	Colour
Number of Photographs	2	3	4	16
Image Size [cm]	23 × 23	23 × 23	23 × 23	23 × 23
Nominal Scale	1:20,000	1:20,000	1:20,000	1:5000
Scanning Resolution [dpi]	1200	1200	1200	1200
Pixel Size [m]	0.42	0.42	0.42	0.11
Waterfront Coverage [km]	6.37	6.99	14.01	14.30
RMSE [m]	1.92	1.94	1.18	0.51

Table 2
Details of the digital images. Source of the data, date, number of images used to make up the photomosaics; pixel size, lineal waterfront coverage of each generated photomosaic and estimated RMSE.

Digital Image	2011	2021
Source	GE	GE
Date	10 Jan 2011	20 Nov 2021
Number of Photographs	10	10
Pixel Size [m]	0.33	0.33
Waterfront Coverage [km]	14.30	14.30
RMSE [m]	0.73	0.69

1600 m × 900 m and resulting in a pixel size of 0.33 m.

Aerial and satellite images were orthorectified and georeferenced (WGS84 - UTM Zone 21 S) by 10 evenly distributed ground control points (GCPs) in order to avoid geometric distortions and the misalignment of photomosaics. For this purpose, real-time kinematic (RTK) GPS/GNSS surveys were carried out during 2022. Two L1/L2/L5 GPS receivers corresponding to the Kolida K7/K58 System. The GCPs were located along reference points such as road intersections, corners of buildings and other infrastructure features common to all the available images. The root mean square error (RMSE) was taken as the accuracy measure to assess the orthorectifying process based on at least 10 points per image. The RMSE is formulated as:

$$RMSE = \sqrt{\frac{\sum_{i=1}^{n} (x_j - x_i)^2 + (y_j - y_i)^2}{n}} \quad , \tag{2}$$

where n is the number of checkpoints, x_j and y_j represent the image coordinates, x_i and y_i represent the checkpoints coordinates. Emerging from the orthorectification process, the RMSE of the images ranged from 0.51 m to 1.94 m (Table 1; Table 2). For each time slice, the images were combined to make up photomosaics covering the study area. The imagery availability did not allow for a complete waterfront coverage throughout the whole time scale. The RMSE adopted for each photomosaic corresponds to that of the image with the highest RMSE (Araujo et al., 2009). The above-mentioned geospatial processing steps were performed using the Esri Geographic Information System (ArcGIS) software (https://www.esri.com/en-us/home).

2.3. Multitemporal shoreline mapping

In order to define the shoreline position, the wet/dry boundary was selected as a shoreline proxy. This feature provides a good estimation of shoreline position under microtidal regimes (Virdis et al., 2012), which is the condition in the study area. Multitemporal shoreline position across the approximately 14 km of waterfront were mapped from the six constructed photomosaics (1965–1975 - 1985–1997 - 2011–2021). This step was conducted by a manual digitization of the shoreline features, supported by ArcGIS software digitization tools.

2.4. Shoreline uncertainty

In order to enhance the shoreline evolution assessment, the uncertainties affecting each shoreline position were estimated. This approach aims to reduce the effect of short-term variability (tides, storms, wave run-up, etc.) and the errors induced by the image acquisition methods over the mid-term analysis. Uncertainties were assumed to be independent, uncorrelated and random, enabling the estimation of the total uncertainty (σT) as (Romine et al., 2009; Virdis et al., 2012; Manno et al., 2017):

$$\sigma T = \pm\sqrt{\sigma_d^2 + \sigma_p^2 + \sigma_r^2 + \sigma_{co}^2 + \sigma_{wr}^2 + \sigma_{td}^2} \quad , \tag{3}$$

where σ_d is the digitization error, evaluated by mapping the same historical shoreline several times and estimating its standard deviation of position residuals for that feature. It depends on the images' brightness, contrast and the ability to accurately visualize the wet/dry boundary; σ_p is the pixel error assumed as the pixel size (equation (1)); σ_r is the orthorectification error, meaning the checkpoints' RMSE of the photomosaics (equation (2)); σ_{co} is the coregistration error resulting from the misalignment between single pixels from the set of images. Some authors consider this error to be equal to the σ_p (Manno et al., 2017); σ_{wr} is the wave run-up error, considered as a short-term effect and based on the extreme run-up elevation R2% (Ruggiero et al., 2001); finally, the σ_{td} is the tidal fluctuation error, taking into account the local tide regime. On the one hand, the σ_{wr} and σ_{td} errors are directly related to geomorphologic and wave climate characteristics of the analyzed beaches; on the other hand, σ_p, σ_r, σ_d and σ_{co} are linked to the images' characteristics and metadata. σ_{wr} and σ_{td} estimation is discussed in the following section.

2.5. Wave climate characteristics

Due to the lack of in-situ data for the study area, the ERA5 dataset of the European Centre for Medium-Range Weather Forecasts (ECMWF) was used in order to estimate the wave climate uncertainties. The ERA5, which replaces the previous ERA-I model, consists of instantaneous forecast values of a global grid re-analysis model with 1-hourly temporal resolution and 0.5° × 0.5° latitude-longitude horizontal resolution (Hersbach et al., 2019). The global wave data quality of the ERA5 model has been validated through buoy and altimeter data analyses (Timmermans et al., 2020).

The wave run-up error (σ_{wr}) can be estimated if the extreme run-up elevation (R2%) is known by field surveys. Due to the lack of monitoring data for our study region, the R2% was predicted by means of empirical equations (Stockdon et al., 2006), which consider the beach slope, the significant wave height (Hs) and the wave period (T). Based on ERA5 monthly averaged data for the 1965–2021 period, we assume a Hs of 0.92 m (Std = 0.11 m) and a T of 6.0 s (Std = 0.5 s). The beach foreshore slope was estimated from previous beach survey data (Bértola et al., 2021) as 5.32% (Std = 1.15%). According to Stockdon et al. (2006) the R2% for natural beaches is estimated by:

$$\mathbf{R2\%} = \mathbf{1.1}\left[\left(\mathbf{0.35\beta}\sqrt{\mathbf{HsL}}\right) + \frac{\sqrt{\mathbf{HsL}\left(\mathbf{0.563\beta^2 + 0.004}\right)}}{\mathbf{2}}\right] \quad , \tag{4}$$

where Hs is the significant wave height, **β** is the beach slope and L is the wavelength. The latter parameter was previously estimated according to Stockdon et al. (2006) as:

$$\mathbf{L} = \frac{\mathbf{gT^2}}{\mathbf{2\pi}} \quad , \tag{5}$$

where g is the gravitational acceleration and T is the wave period taken from the deep-water ERA5 time-series data. Finally, the σ_{wr} was calculated following Manno et al. (2017) as:

$$\boldsymbol{\sigma_{wr}} = \frac{\mathbf{Std_{R2\%}}}{\boldsymbol{\beta}} \quad , \tag{6}$$

where $Std_{R2\%}$ is the standard deviation of the R2% estimated by equation (4), and **β** is the beach slope.

In order to estimate the tidal fluctuation error (σ_{td}) the local tide records were modelated based on the widely used (Byun and Hart, 2019) T_Tide as a MATLAB ® package for harmonic analysis and tide predictions developed by Pawlowicz et al. (2002). As well as for the estimation of the wave run-up, the 3-hourly tide records were modeled for the 1965–2021 period assuming a mean value of 0.902 m and a standard deviation of 0.236 m, with a mean tide range of 0.668 m. As proposed in equation (6), the σ_{td} was calculated as (Manno et al., 2017):

$$\boldsymbol{\sigma_{td}} = \frac{\mathbf{Std_{TD}}}{\boldsymbol{\beta}}, \tag{7}$$

where Std_{TD} is the standard deviation of the mean tide emerging from the T-Tide modeling, and **β** is the beach slope. This allowed the estimation of shoreline change rates through the transect based analysis (TBA) (Anfuso et al., 2016). It was applied taking into account 288 shore-normal transects spaced every 50 m in a south-north way.

2.6. Shoreline evolution assessment

The delimitation of multitemporal shoreline positions and the estimation of its associated uncertainties allowed the subsequent assessment of shoreline change rates. For this purpose, a transect based analysis was conducted (Anfuso et al., 2016) by 288 shore-normal transects spaced every 50 m in a south-north way. The shoreline position measurements were referenced using the baseline method (Leatherman and Clow, 1983) linked to an arbitrary baseline vector located offshore. This determined that the positive values meant accretion processes and the negative values erosion processes.

Based on this, four shoreline change (NSM, SCE, EPR, WLR) statistics were estimated for each transect by using the DSAS v5.0 tool (Himmelstoss et al., 2018) within the ArcGIS graphical user interface environment. The main characteristics of each result statistic are detailed in Table 3. In addition, the beach width was estimated taking into account the shoreline and the foredune foot positions for each image (Virdis et al., 2012). In those cases where the foredune foot was artificially eliminated, the coastal promenade was delimited instead. Finally, a shoreline position forecast up to 2030 was driven by extrapolating the estimated EPR of the latest studied period (2011–2021).

All the statistics results were smoothed by averaging the rates alongshore with the use of a weighted five-transect-sliding filter as proposed in Fletcher et al. (2003). The absence of artificial surfaces, infrastructure or defense structures allowed the definition of a continuous shoreline.

In order to generate a zonification of the study area, the entire waterfront was divided into 29 sectors from south to north. Each of them comprised 10 transects (500 m) and was analyzed on the basis of the WLR and average beach width. The latter was defined as the arithmetic mean of the average beach width of every transect on the sector. Finally, the presence of EHS was defined on the basis of the WLR parameter as an area with an average WLR lower than −0,3 m/yr for at least two consecutive sectors (1 km). The shoreline delimitation and the geospatial data processing were carried out by the users' graphical interface of the ArcGIS software including the DSAS tool (v5.0).

Table 3
Detail of the statistics results computed in this work. NSM, SCE, EPR and WLR were estimated within the framework of the DSAS tool.

Result Statistic	Concept	Measurement Unit
Net Shoreline Movement [NSM]	Distance between oldest and more recent shoreline position	m
Shoreline Change Envelope [SCE]	Greatest distance among shorelines	m
End Point Rate [EPR]	NSM divided into the time elapsed between oldest and more recent shoreline position	m/yr
Weighted linear regression rate-of-change [WLR]	Temporal best fit regression to all data weighted by shoreline uncertainties	m/yr
Beach Width (Virdis et al., 2012)	Distance between shoreline and foredune foot position	m
Shoreline Forecast 2030	Shoreline position emerging from 2011 to 2021 EPR extrapolation by 2030	m

3. Results

3.1. Shoreline positional uncertainties

In order to obtain the total uncertainty (σ_T) estimation (Table 4), those errors linked to the image's acquisition characteristics and metadata were estimated: the digitization error (σ_d) was estimated between 1.63 and 3.84 m; the pixel error (σ_p) and the coregistration error (σ_{co}) (see equation (1)) showed values between 0.11 and 0.42 m; and the orthorectification error (σ_r) resulting from the checkpoints' RMSE (see equation (2)) ranged from 0.51 to 1.94 m. At the same time, those errors related to geomorphologic and wave climate characteristics of the study zone were also calculated: the R2% was estimated as 0.44 m (Std = 0.07 m) resulting on a wave run-up error (σ_{wr}) of 1.27 m (see equations (4)–(6)); the mean tide record was 0.90 m (Std = 0.24) and the tidal fluctuation error (σ_{td}) was calculated as 4.43 m emerging from equation (7). Finally, on the basis of equation (3), the total shoreline delimitation uncertainty (σ_T) ranged from ±5.06 m in 1985 to ± 6.02 m in 1997 (Table 4; Fig. 2).

3.2. Shoreline evolution (1965–2021)

The waterfront coverage of the photomosaics only allowed a full shoreline analysis (288 transects) for the 1985–2021 period. However, in the 1965–2021 period, 131 transects were analyzed by 6 shoreline positions, while in the 1975–2021 period 143 transects were computed for 5 shoreline positions. The analysis showed, for 1965–2021, an average NSM of −14.6 m, with a maximum erosion transect (MET) of −44.8 m (n° 200) and a maximum accretion transect (MAT) of 27.1 m (n° 266). Between 1975 and 2021 shorelines, the average NSM was −4.3 m, with a MET of −41.1 m (n° 167) and a MAT of 32.1 m (n° 255). Finally, for the 1985–2021 period, the average NSM was −10.8 m, with a MET of −43.1 m (n° 201) and a MAT of 34.7 m (n° 281). The maximum SCE transect value was 62.5 m for the three considered periods; the minimum SCE values for 1965–2021, 1975–2021 and 1985–2021 periods were 17.9 m, 17.3 m and 4.79 m respectively (Fig. 3).

Table 4
Total shoreline mapping uncertainty for each time span (units in meters).

Uncertainties	1965	1975	1985	1997	2011	2021
σ_d	2.33	1.98	1.63	3.84	2.73	2.54
σ_p	0.42	0.42	0.42	0.11	0.33	0.33
σ_r	1.92	1.94	1.18	0.51	0.73	0.69
σ_{co}	0.42	0.42	0.42	0.11	0.33	0.33
σ_{wr}	1.27	1.27	1.27	1.27	1.27	1.27
σ_{td}	4.43	4.43	4.43	4.43	4.43	4.43
σ_t	5.54	5.41	5.06	6.02	5.43	5.33

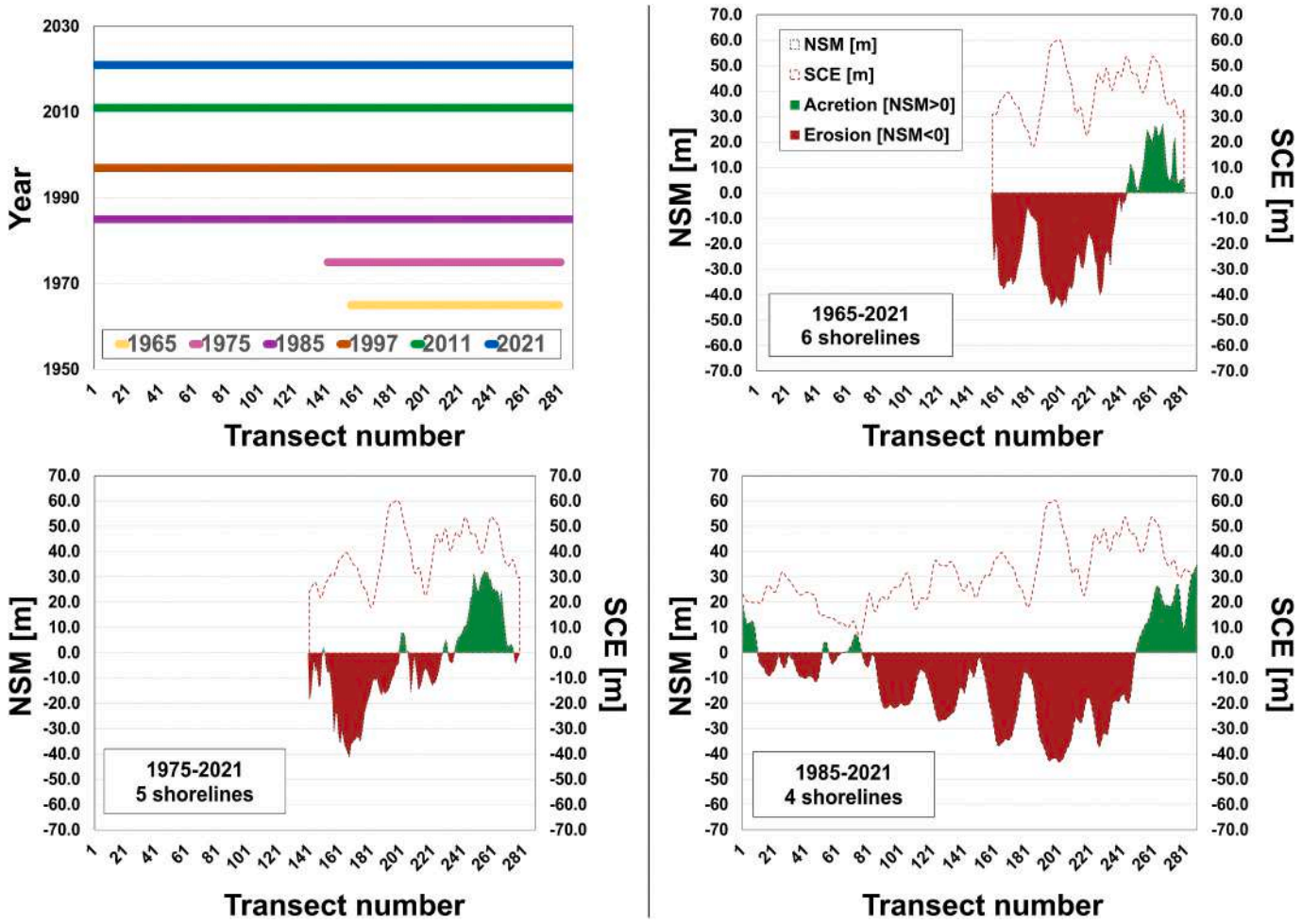

Fig. 3. NSM and SCE for the 1965–2021, 1975–2021 and 1985–2021 periods. Top left: waterfront coverage and temporal separation between the six shorelines used in this study,

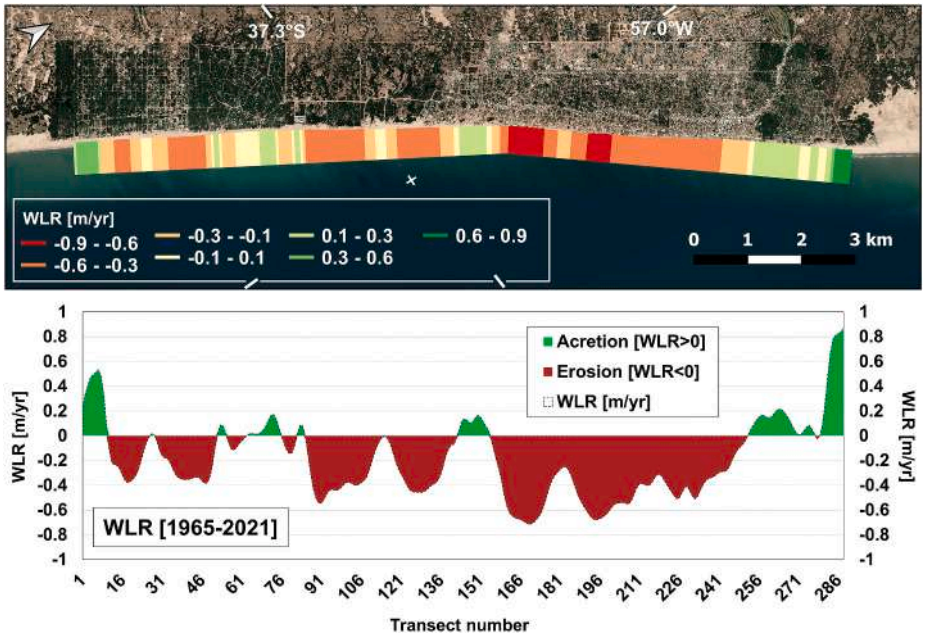

Fig. 4. WLR [1965–2021] values for the 288 analyzed transects. Background image corresponds to the Google Satellite QuickMapService basemap for ArcGIS software.

The WLR, obtained by taking into account the shoreline uncertainties, showed an average value of −0.20 ± 0.47 m/yr with a MAT of 0.871 m/yr and a MET of −0.713 m/yr (Fig. 4). 72.1% of the transects showed negative values with an average of −0.346 m/yr while the remaining showed an accretional average value of 0.186 m/yr.

In order to generate a zonification of the study area, the average WLR and the average beach width were estimated for each sector (Fig. 5). The maximum average WLR was 0.631 m/yr (sector n° 29) and the minimum was −0.664 m/yr (sector n° 17). 7 sectors presented positive WLR values (accretion) while the remaining 22 sectors presented negative WLR values (erosion). The average for the accretional sectors was 0.202 m/yr; the average for the erosional sectors was −0.326 m/yr. The beach width ranged from 54.54 m (sector n° 22) to 143.19 m (sector n° 29) with an average value of 88.54 m. 19 sectors presented beach width values below 100 m.

These results allowed us to identify five zones (Fig. 5): Las Gaviotas/Mar Azul zone (sectors 1 to 4), Mar de Las Pampas zone (sectors 5 to 8), Southern Villa Gesell zone (sectors 9 to 15), Villa Gesell Midtown (sectors 16 to 25) and Northern Villa Gesell zone (sectors 26 to 29).

3.2.1. Zone A - Las Gaviotas/Mar Azul

This zone included sectors 1 to 4 with a linear waterfront coverage of 2 km and comprised the homonymous coastal villages. It represented the transition from an erosional to an accretional coast in a N–S direction (Fig. 6). Three of its sectors showed negative WLR values with an average of −0.242 m/yr and a maximum of −0.340 m/yr; the southernmost sector showed an accretional WLR average of 0.429 m/yr. The average beach width varied between 110.6 m in 2011 and 133.9 m in 1985. The maximum beach width was registered as 160.2 m in 2021 and the minimum was 91.0 m in 2011. Taking into account the average EPR value, the maximum erosional period was 1985–1997 with −0.97 m/yr while the maximum accretional period was 2011–2021 a value of 1.90 m/yr. The NSM represented an average value of −1.2 m, with a maximum of 19.9 m and a minimum of −10.0 m. 58% of the transects showed erosional NSM values, all of them located in the northern area of this zone. The SCE values ranged between 17.2 and 34.0 m.

3.2.2. Zone B - Mar de Las Pampas

This zone was delimited between sectors 5 and 8 including Mar de Las Pampas village (Fig. 7). It showed a transition from shorter to wider and from stable to erosional beaches in a N–S direction. The average beach width ranged from 80.3 m in 1997 to 90.8 m in 1985. The maximum beach width was observed in 1985 (161.1 m) while the minimum in 1997 (52.3 m). The average WLR value was −0.009 m/yr, which denotes a stable coastline over time. The maximum erosional EPR period was 1985–1997 (−0.83 m/yr); the maximum accretional EPR period was 2011–2021 with a value of 0.81 m/yr. The average NSM showed a value of −2.0 m, with a maximum of 7.3 m and a minimum of −11.3 m. 60% of the transects showed erosional values, most of them located in the transition towards the Las Gaviotas/Mar Azul zone. The SCE ranged between 4.8 and 24.5 m.

3.2.3. Zone C - Southern Villa Gesell

This zone was delimited between sectors 9 and 16 including Colonia Marina village and the southernmost sector of Villa Gesell city. It showed an erosional coastline over time with an alternation of wider and shorter beaches alongshore. The average beach width was estimated between 93.2 m in 2021 and 117.76 m in 2011. The maximum beach

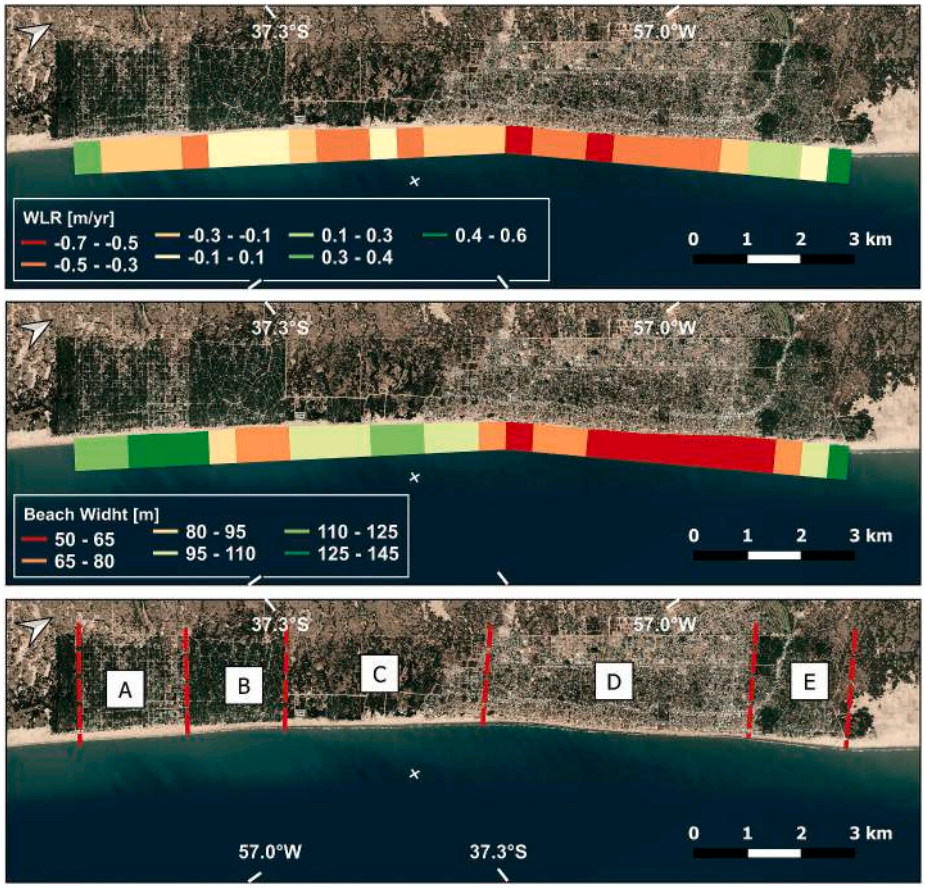

Fig. 5. Average WLR (top) and average beach width (mid) for the 29 sectors. Red-dotted lines indicate the five delimited zones (bottom): Las Gaviotas/Mar Azul (A), Mar de Las Pampas (B), Southern Villa Gesell (C), Villa Gesell Midtown (D) and Northern Villa Gesell (E). Background image corresponds to the Google Satellite QuickMapService basemap for ArcGIS software.

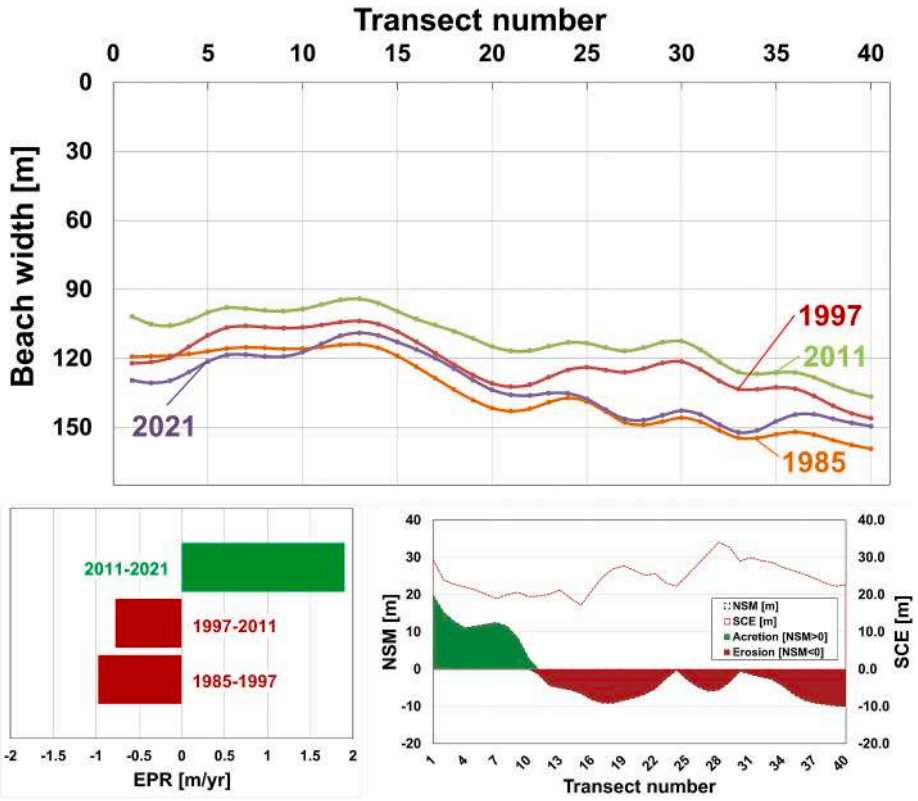

Fig. 6. Top: beach width for the four shoreline positions. Bottom left: end-point rate for the three studied periods. Bottom right: net shoreline movement (1985–2021) and shoreline change envelope for the 40 transects included in the Las Gaviotas/Mar Azul zone.

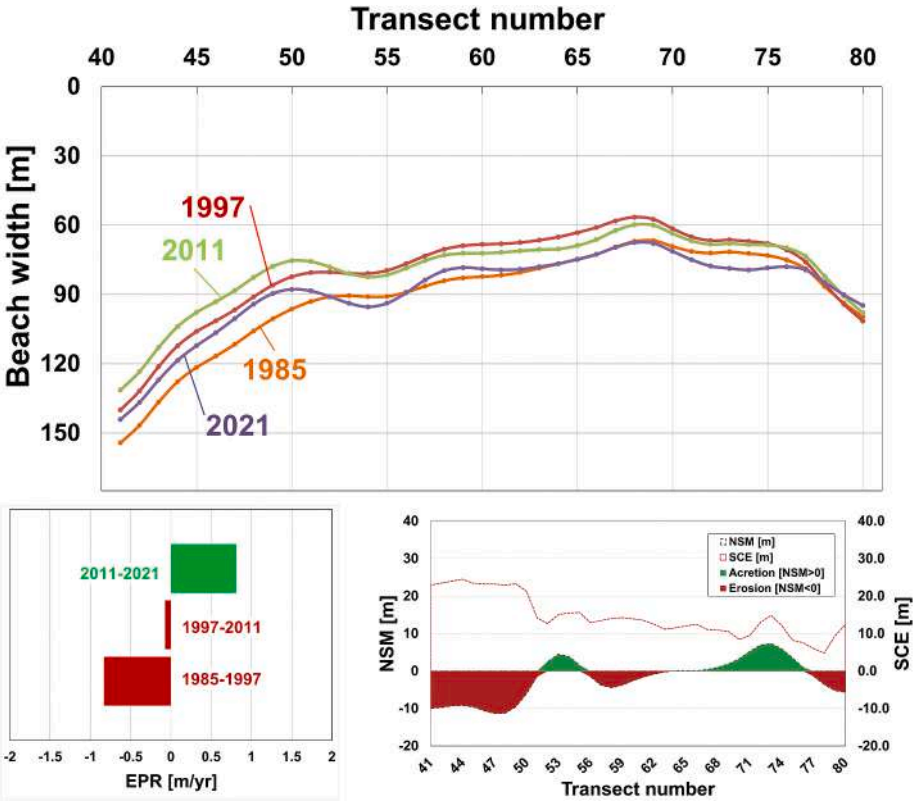

Fig. 7. Top: beach width for the four shoreline positions. Bottom left: end-point rate for the three studied periods. Bottom right: net shoreline movement (1985–2021) and shoreline change envelope for the 40 transects included in the Mar de Las Pampas zone.

width value was observed in 2011 (159.8 m) and the minimum in 2021 (59.6 m). The average WLR value was −0.249 m/yr. The EPR ranged from −2.26 m/yr (2011–2021 period) to 1.08 m/yr (1997–2011 period). The average NSM was −16.1 m (Min = −26.9 m; Max = −0.7 m) with the 100% of the transects associated with erosional values. The SCE ranged between 12.4 and 38.3 m (Fig. 8).

3.2.4. Zone D - Villa Gesell Midtown

The Villa Gesell Midtown zone comprised 10 sectors (16–25) with a linear waterfront coverage of about 5 km. It represented the highest erosional coast and the narrowest beaches of the study area. 80% of this one meets the defined criteria to be considered an EHS (sectors 18 to 25). It showcases a wide array of anthropic modifications of the littoral environment, including a dock, the placement of beach facilities on the coastal dunes, and even the complete removal of the foredune. The average WLR value was estimated as −0.422 m/yr and the average NSM as −25.8 m (Max = −1.2 m; Min = −43.1 m). The 100% of the transects showed erosional NSM values. The maximum erosional EPR was the 1965–1975 period (−1.35 m/yr) while the only accretional EPR period was 1997–2011 (0.23 m/yr). The 2011–2021 period showed a non-significant change rate of about 1 cm/yr. The average beach width ranged from 50.5 m in 1997 to 78.4 m in 1965. The maximum beach width was registered in 2011 (98.5 m) while the minimum was 31.5 in 1997. The SCE values ranged between 15.2 and 62.5 m (Fig. 9).

3.2.5. Zone E – Northern Villa Gesell

This zone comprised sectors 26 to 29 and represented an accretional coast with the highest beach width values of the study area (Fig. 10). At the same time, it represented a transition from the shorter to wider beaches in a S–N direction. The average beach width ranged from 69.7 m in 1997 to 110.1 m in 2021. The shortest beach was observed in 1997 (30.9 m) while the widest in 2021 (163.6 m). The average WLR value was 0.221 m/yr, which denotes an accretional coastline for the studied period. This zone showed 3 erosional EPR periods (1965–1975, 1975–1985 and 1985–1997) with values of −0.39, −0.59 and −1.49 m/yr respectively. However, 1997–2011 and 2011–2021 periods represented important accretion conditions with 1.61 and 1.79 m/yr respectively. The NSM showed only accretional transects; the average value was 19.31 m, with a maximum of 34.70 m and a minimum of 4.29 m. The SCE ranged between 27.6 and 56.4 m.

3.3. Shoreline forecast

Based on the shoreline position forecast, the beach width was estimated by considering the year 2030 as time horizon (Fig. 11). The average beach width for the study area was almost stable between 2021 (86.25 m) and 2030 (87.34 m). However, the forecast results were different between zones: three of them showed an accretional tendency, one of them a highly erosional tendency and the remaining was almost stable through the predicted time lapse.

The Las Gaviotas/Mar Azul zone showed a net movement of 17.14 m, representing an average beach width of 149.21 m for 2030 (Max = 163.18 m; Min = 140.03 m) (Fig. 12); the Northern Villa Gesell zone showed an accretional net balance of 16.11 m, representing an average beach width of 124.98 m for the same year (Max = 159.32 m; Min = 97.15 m); and the Mar de Las Pampas zone average beach width was calculated as 95.17 m (Max = 119.01 m; Min = 80.99 m) resulting from a positive net movement of 7.29 m. In contrast, the Southern Villa Gesell zone showed a net movement of −20.43 m resulting in an average beach width of 72.37 m (Max = 93.62; Min = 55.41 m) (Fig. 12). Finally, the Villa Gesell Midtown zone showed a net movement of −0.09 m resulting in an average beach width of 53.72 m (Max = 72.22 m; Min = 41.41 m).

4. Discussion

The results of this study evidenced contrasting zones with distinct

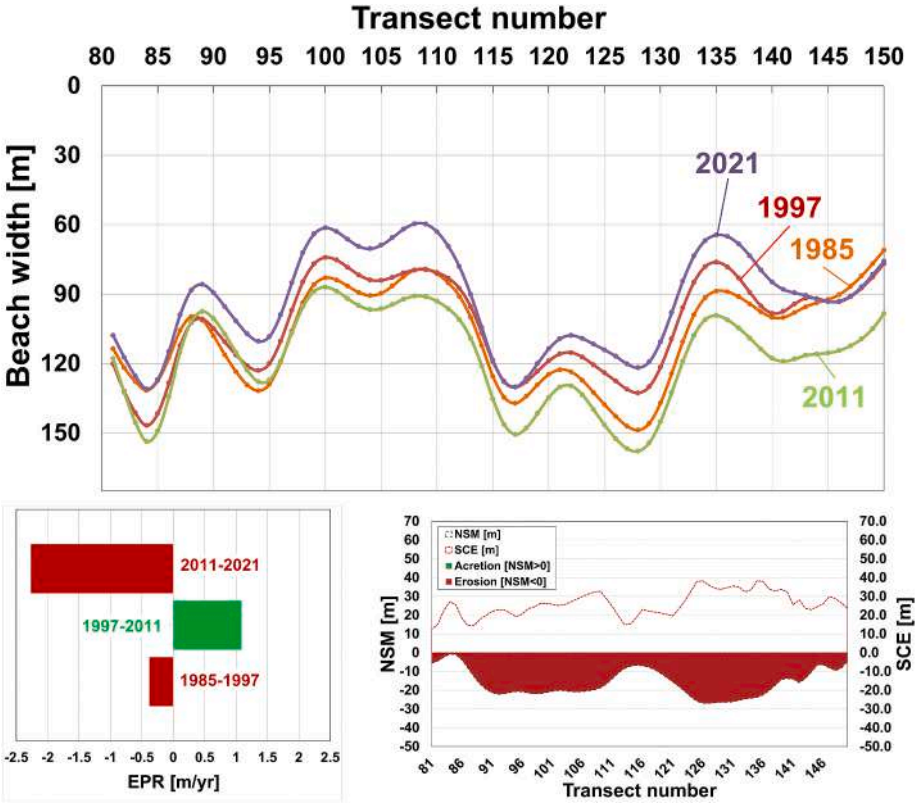

Fig. 8. Top: beach width for the four shoreline positions. Bottom left: end-point rate for the three studied periods. Bottom right: net shoreline movement (1985–2021) and shoreline change envelope for the 70 transects included in the Southern Villa Gesell zone.

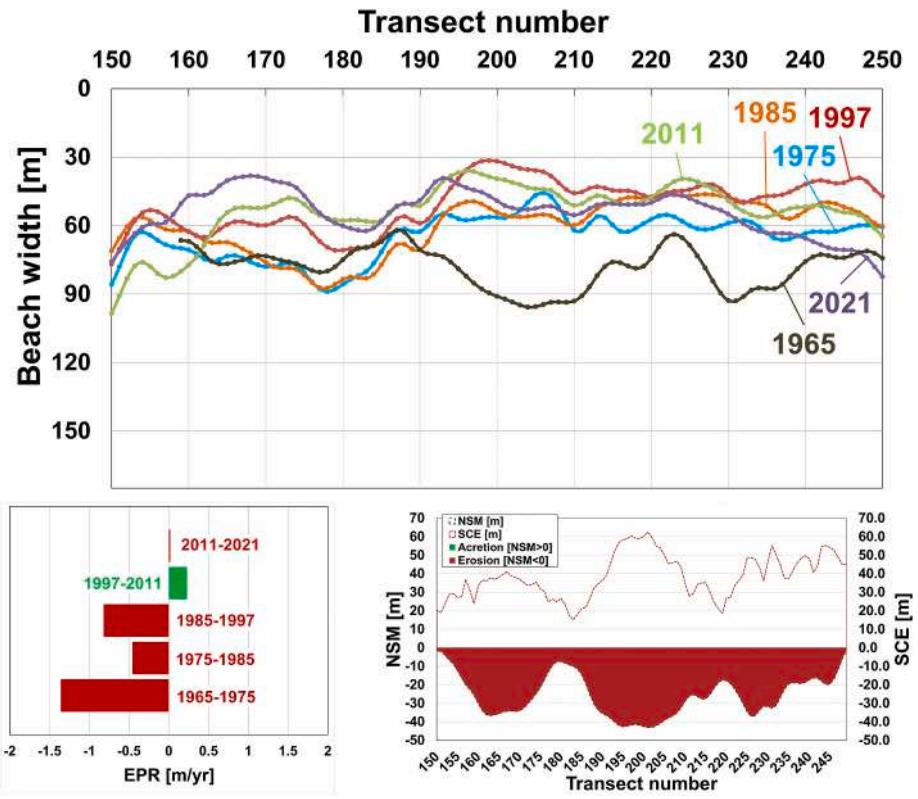

Fig. 9. Top: beach width for the six shoreline positions. Bottom left: end-point rate for the five studied periods. Bottom right: net shoreline movement (1965–2021) and shoreline change envelope for the 100 transects included in the Villa Gesell Midtown zone.

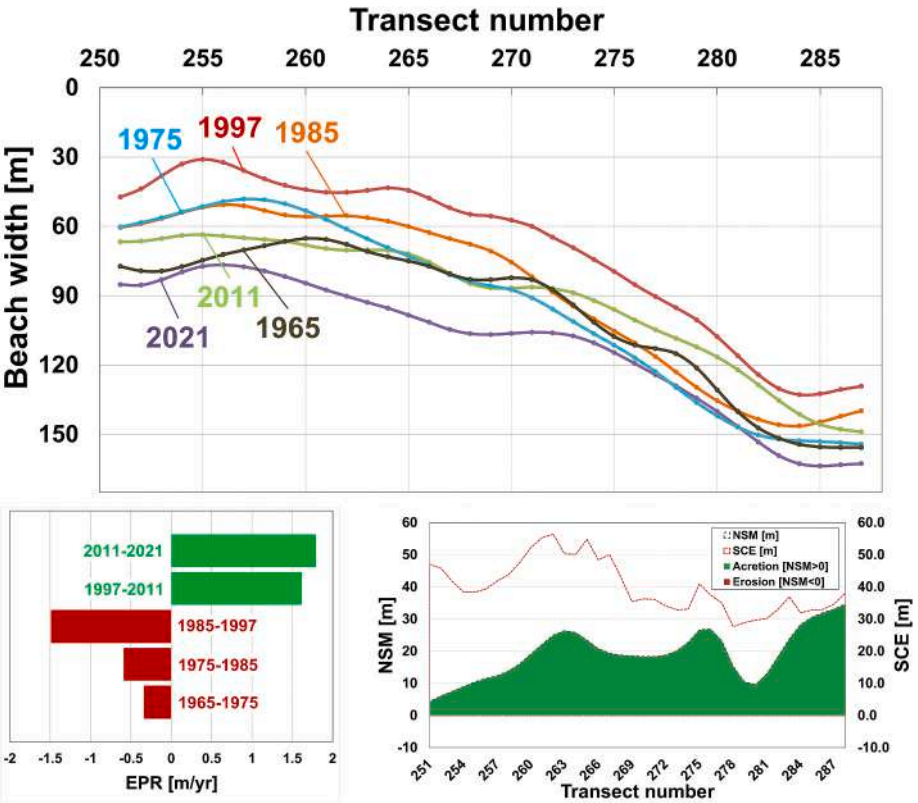

Fig. 10. Top: beach width for the six shoreline positions. Bottom left: end-point rate for the five studied periods. Bottom right: net shoreline movement (1965–2021) and shoreline change envelope for the 38 transects included in the Northern Villa Gesell zone.

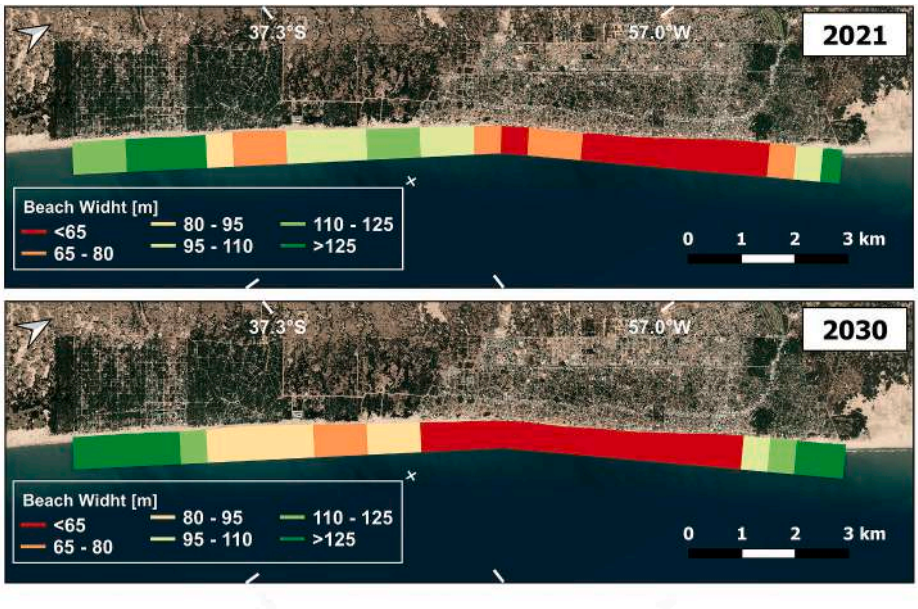

Fig. 11. Observed (2021 - top) and forecasted (2030 - bottom) beach width based on the shoreline change forecasting. Background image corresponds to the Google Satellite QuickMapService basemap for ArcGIS software.

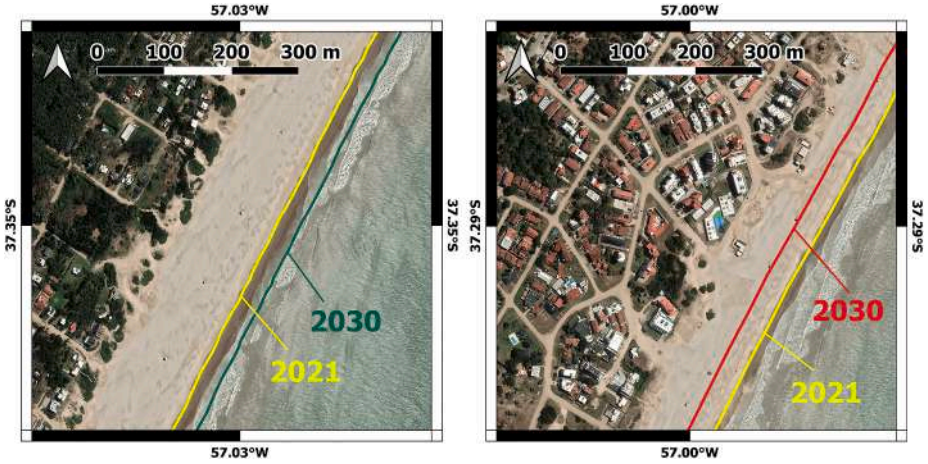

Fig. 12. Forecasted shoreline change between 2021 and 2030 for Las Gaviotas/Mar Azul zone (left) and Southern Villa Gesell zone (right). Background image corresponds to the 2021 orthorectified photomosaic (see Table 2).

patterns of change and observed differences in erosion/accretion balances. These results are consistent with previous studies conducted for this coastline sector (Marcomini and López, 1997; Isla et al., 1998; Bértola et al., 1999; Bértola, 2006; Isla et al., 2018; Bértola et al., 2021).

Emerging from the WLR parameter, the ~70% of the shoreline presented erosional rates. In addition, an EHS was identified representing the ~80% of the Villa Gesell Midtown zone and the ~30% of the study area. This characterization of critical zones represents the first milestone of a line of research that could ultimately provide a comprehensive assessment of beach morphodynamics in the coast of Villa Gesell. Following that line, two important and interconnected issues arise: (1) the distinction between natural and anthropogenic factors conditioning the occurrence and location of the EHS, and (2) the evaluation and, if possible, quantification of cross-shore and along-shore processes controlling local coastal dynamics.

Regarding the first issue, it is well accepted that nearshore bathymetry and its influence over wave energy and circulation has an impact on beach and sandbar morphology (Wright and Short, 1984; Wright, 1995; Komar, 1998; Plant et al., 2001; Bose et al., 2020). This effect has been suggested by previous work on the coast of Villa Gesell (Bértola, 2006), but has not been thoroughly assessed. Some processes affecting local sediment budgets (e.g., alongshore variations in sediment transport, variations in the delivery and storage capacity of sources and sinks over time) can be difficult to quantify, and in some cases, alongshore variability of shoreline change in relatively straight sandy beaches still remains poorly understood (Fenster and Dolan, 1993). Alves (2009) explained the occurrence and behavior of an EHS in the southern sandy coast of Brazil through coastal instability (induced by wave obliqueness) and sediment transport analysis. A multi-proxy approach that incorporates numerical modeling and the acquisition of bathymetry and beach topography data would be optimal for addressing this series of factors.

The second issue becomes particularly important when considering the role of anthropogenic activities over the development of an EHS. Martín Martín Prieto et al. (2018) obtained, in the southern beaches of Mallorca (Spain) and for the period 1956–2015, WLR rates between −0, 38 and 0,29 m/yr. The higher erosional rates were found in locations affected by human activities, such as parking lots, access points for

tourism and earthmoving machinery, etc. Cellone et al. (2016) determined, in a storm-dominated marshland in the Rio de La Plata estuary (Argentina), an average WLR of −0,4 m/yr, with the highest erosional values being up to −7,4 m/yr. The latter were linked to the removal of native vegetation, as in these tidal environments, the vegetation acts as a stabilizer of the fine sediment that forms the marshland, and therefore its removal promotes higher erosion scenarios during storm events. These studies provide further evidence supporting the concept proposed by Clark (1997) that LULC changes have significant impacts on coastal areas worldwide. The Villa Gesell shoreline evolution analysis regarding these changes is discussed below.

The results of this study allowed us to associate each zone's evolution with different historical LULC. Since 1930, a total of ~1700 ha corresponding to zones C, D, and E, have undergone intensive dune fixation processes using rapid-growth exotic tree species (Juárez and Mantobani, 2006). In zones A and B, a similar dune fixation approach was not implemented until the 1980s, covering an area of ~1400 ha.

In Zone D (Villa Gesell City midtown), the dune stabilization allowed the establishment of asphalted streets, buildings and other urban features. Furthermore, foredunes were eliminated to construct a coastal promenade and bathing facilities. This zone encompasses the EHS defined in the present work, which would imply that local cross-shore imbalances are heavily responsible for the high erosion rates of these beaches. However, the influence of alongshore imbalances due to dune fixation and updrift modification of the sediment budget shouldn't be discarded (Isla et al., 1998). Moreover, the implementation of higher resolution field surveys could provide a useful insight about the role of very specific interventions (such as urban storm drains) over the development of a larger erosional hot spot.

The remaining zones were mainly affected by the afforestation processes, but with significantly lower urbanization trends; foredune was conserved, streets were not asphalted and urban expansion was driven by residential villages instead of dense building zones. Erosional rates were lower and even accretional sectors were identified. Zones A, B and E, despite showing erosion during the first stages of its afforestation process, are now representing an accretional coast. LULC changes could have promoted wider beaches over these zones (Fig. 13).

In zones D and E those balances related to 1997–2011 and 2011–2021 periods showed different trends related to previous ones. In 2006, based on several damages caused by coastal erosion, the Villa Gesell Government carried out the Integrated Coastal Management Plan (Plan de Manejo Integrado del Frente Costero de VIlla Gesell - Ordinance N° 2050/06). It implied, among other policies, the replacement of the coastal promenade built by 1981 and the bathing facilities (called "balnearios"). These changes represented the increase of the accretional rates for zone E and the transition from an erosional to an accretional coast. A beach recovery was identified during 1997–2011 for zone D, which represented its only accretional period. However, the 2011–2021 period was associated with erosional trends as before these management policies were implemented (Fig. 14).

In addition, the shoreline position forecasted up to 2030 provided an estimation based on the more recent shoreline change rates observed for each sector. Future LULC changes of the coastal zone could have a negative or positive impact on these rates. The Villa Gesell Assessment Plan for Coastal Urbanization (Plan de Ordenamiento Municipal; Decree No. 13621/21) proposes an increase in the tourist population of about 200% for 2045. To this end, it is proposed to extend the developable waterfront in 9 km and to expand the urban sprawl in about 1300 ha. The execution of the research lines derived from this contribution could be crucial for the implementation of this urbanization plan.

In order to support the obtained results, several methodological aspects deserve to be discussed. Regarding the geospatial analysis, it was mainly limited by the aerial photographs availability and its waterfront coverage (Table 1). The assessment of the entire Villa Gesell shoreline was only possible for the 1985–2021 period by the implementation of 288 transects (~14,5 km). In contrast, for the 1965–2021 and 1975–2021 periods, 131 (~6,5 km) and 143 (~7 km) transects were obtained, respectively. This resulted in a lack of evidence between 1965 and 1985 for the shoreline corresponding to zones A, B and C principally (Fig. 3). Other remote sensing techniques such as optical band-combination methods can be used (Nassar et al., 2018), however, these techniques significantly reduce the time span of the analysis due to the lesser availability of historical data.

The 1997 aerophoto showed the highest overall uncertainty value ($\sigma_T = 6.02$ m) due to the greatest digitization error ($\sigma_d = 3.84$ m). This error is linked to some images' characteristics which define the feasibility of shoreline delimitation through the selected proxy, the digitization tool configuration (e.g. line thickness), and the experience of the operator (Moore, 2000). The pixel size was obtained from aerial photographs' nominal scale (1:20,000 and 1:5000). According to Moore (2000) these are the optimal scales for shoreline delimitation studies. Blount et al. (2022) propose to consider the digitization (σ_d) error equal to pixel error (σ_p). Sensors such as TM and ETM+ from Landsat 5 and 7 missions, respectively, have a pixel spatial resolution of about 30 m for optical bands. This reinforces the advantages of using aerial photographs by manual digitization methods over multiespectral automatic or semi-automatic techniques.

The wet/dry boundary is widely used and considered as a practical solution to identify shoreline position (Pajak and Leatherman, 2002), but it is also questioned due to its stational variability and sometimes

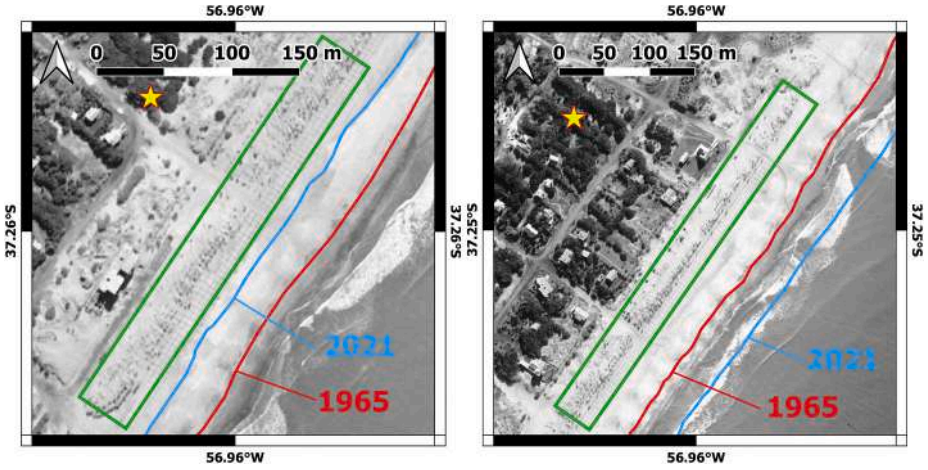

Fig. 13. Shoreline position for 1965 and 2021 in zones D (left) and E (right). The image corresponds to the 1965 orthorectified photomosaic (see Table 1); the green rectangle indicates zones of foredune fixation by exotic plant species; the yellow star indicates the original afforestation processes carried out since the '30s.

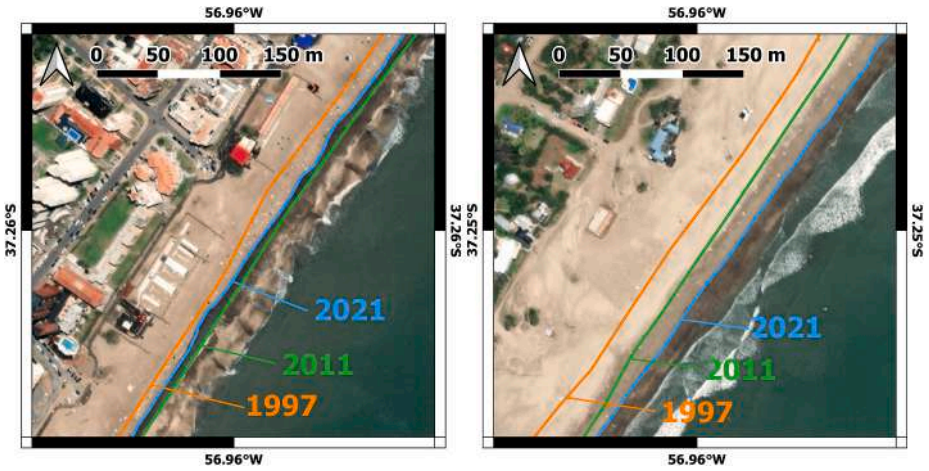

Fig. 14. Shoreline position for 1997, 2011 and 2021 in zones D (left) and E (right). In 2006, the Villa Gesell government carried out different management policies throughout the waterfront of these zones. Background image corresponds to the 2021 orthorectified photomosaic (see Table 2).

low visibility in satellite images (Moore, 2000). It is affected by astronomical tides, seasonal beach changes, storm events, and wind tides (Pajak and Leatherman, 2002). However, the effect of these variables is reduced when dealing with a larger time scale such as the 1965–2021 period of this study (Crowell et al., 1993; Muehe and Klumb-Oliveira, 2014). In addition, the error provided by high tide and wave action in aerial photographs and satellite images is covered by tide and run-up errors estimation (Moore, 2000).

The lack of in situ wave climate data has led to the use of modeled and reanalysis data. While this information has been validated and widely used (Timmermans et al., 2020), it may not include information about factors and processes that condition the specific coastal dynamics (eg. near-shore bathymetry). For this study, tidal fluctuation represented the greatest source of error ($\sigma_{td} = 4.43$ m) even representing a microtidal coast. In contrast, Virdis et al. (2012) obtained $\sigma_{td} = 1.5$ m for the coast of Sardinia, Italy, based on in situ measurements.

Regarding the shoreline forecasting method, the DSAS v5.0 includes a widely used tool for this purpose based on the WLR rate (Apostolopoulos and Nikolakopoulos, 2020; Apostolopoulos et al., 2022 Cellone et al., 2016; Chrisben and Gurugnanam, 2022; Al-Ruheili and Boluwade, 2021). In a general context, with no information about the factors conditioning the specific coastal dynamics, such a method would be appropriate. However, the analysis presented in this work shows a direct influence of anthropogenic activity over coastal dynamics, and some of the changes observed in the erosion/accretion rates of the identified zones can be linked to specific modifications of the dune-beach system carried out by the local administration. Therefore, the EPR of the last period (2011–2021) is considered to reflect the coastal dynamics under the current geomorphological and anthropogenic conditions, and thus provide a better estimation for shoreline evolution in the near future. In this situation, the exception to using the longest term data should be the right approach (Crowell et al., 1993).

Despite these method considerations, the σ_T values corresponding to the six delimited shorelines ranged from 5.06 to 6.02 m (Table 4), being below the approximate average of uncertainty (10 m) proposed by the National Assessment of Shoreline Change Project, estimated by the U.S. Geological Survey (USGS) (Himmelstoss et al., 2018). This demonstrates the validity of this study in identifying erosion/accretion balances and critical sectors (EHS). Moreover, the correlation between these findings and the LULC changes and historical coastal policies further emphasizes its significance regarding the near-future coastal management actions.

5. Conclusions

This paper presents a medium-term evolution assessment of a linear shoreline sector within a coastal barrier system for the 1965–2021 period. It represents the first study to approach the shoreline evolution for urban and peri-urban beaches of the Villa Gesell County, located in the Eastern Barrier of Buenos Aires, Argentina.

The results showed an average shoreline retreat of ~15 m and an average weighted rate-of-change of −0.2 m/yr for the study area. However, the studied coastline evidenced pronounced along-shore variations in its erosion/accretion balances. The most erosional and the most accretional sectors represented WLRs of −0.664 and 0.631 m/yr, respectively. The proposed zonification allowed for the identification of these contrasting shoreline sectors.

In a S–N direction, the Las Gaviotas/Mar Azul zone represented the transition from accretional to slightly erosional beaches with the highest average beach width of the study area; the Mar de Las Pampas zone showed the transition to narrower and more stable beaches while the Southern Villa Gesell zone represented the beginning of an erosive coast with the alternation of wider and narrower beaches alongshore. Villa Gesell Midtown showed the highest erosional and narrowest beaches of the study area, followed by a transition to an extremely accretional coast (Northern Villa Gesell) with the highest beach width values of the study area.

Despite these along-shore differences, more than 70% of the urban and peri-urban beaches of Villa Gesell showed an erosional balance with an average retreat rate of ~35 cm/yr for the 1965–2021 period. This led to the identification of an erosional hot spot covering ~80% of Villa Gesell Midtown and ~30% of the urbanized waterfront of the county. The remaining represented cumulative beaches with an average rate-of-growth of ~19 cm/yr.

The 2030 shoreline forecast evidenced accretional tendencies between ~7 and ~17 m for peri-urban beaches (Zones A, B and E). Furthermore, urban beaches of zone C suggest a worrying scenario with ~20 m of shoreline retreat indicating the potential development of an erosional hot spot. Zone D represents an almost stable behavior through the predicted lapse.

These results are directly linked to the historical land use/land cover changes of Villa Gesell county which are mainly related to dune stabilization processes and to the implantation of urban surfaces. Zone D, with the most intense development, represented an erosional hotspot which could be mainly caused by local cross-shore imbalances due to these anthropogenic disturbances. However, the impact of alongshore imbalances should not be discarded. In the remaining zones LULC changes could even have promoted wider beaches. In addition, the replacement of the coastal promenade in 2006 led to an increase of accretional rates in Zone E, and even in a beah-recovery period for Zone D.

Despite the method limitations, the shoreline positional uncertainties were better than the recommended parameters, validating the obtained results. These results were constrained by the availability of historical imagery and the absence of in situ wave climate data for the XX century. However, it is suggested that future research should consider shoreline evolution under extreme conditions (storm surge, maximum high tides) in order to enhance the understanding of coastal system dynamics and the role of natural and anthropogenic processes.

Future modifications of the coastal zone could lead to an increase of the erosional rates. The Villa Gesell Assessment Plan for Coastal Urbanization proposes the urban waterfront extension over natural dune areas. The correlation between the results of this work and the historical LULC changes suggests worrying scenarios for these near-future programes. Moreover, the necessity of an integrated coastal zone management framework is reinforced.

This work represents a first step into a comprehensive assessment of an erosional hotspot in a sandy barrier system in Buenos Aires, Argentina. This will allow the developing of future research lines that aim to understand the coastal system dynamics and the role of natural and anthropogenic processes. At the same time, it will support monitoring processes considering the implementation of higher resolution field surveys.

Funding

This study was funded by the Ministry of Science, Technology and Innovation of Argentina trough the project "Topografía, escurrimiento superficial y monitoreo de playas en el Partido de Villa Gesell, Provincia de Buenos Aires" (Impact.AR N° 106 - Dr. F. I. Isla - RESOL-2022-224-APN-SACT#MCT).

CRediT authorship contribution statement

Pedro Andrés Garzo: Software, Resources, Methodology, Investigation, Conceptualization, Funding acquisition, Visualization, Writing - original draft, Writing - review & editing. **Leonardo Sánchez-Caro:** Validation, Resources, Methodology, Investigation, Conceptualization, Funding acquisition, Writing - original draft, Writing - review & editing. **Marcia Mojica:** Investigation, Writing - original draft, Writing - review & editing.

Declaration of competing interest

The authors declare that they have no known competing financial interests or personal relationships that could have appeared to influence the work reported in this paper.

Data availability

Data will be made available on request.

Acknowledgements

The authors acknowledge the Secretary of Culture of the Villa Gesell County for the information about urban historical development.

References

Abreu, M.M.R., Ferro, I.M.M., Abreu Neto, J.C., 2016. Variação e modelo de tendência da linha da costa da Praia do Icaraí.Caucaia, Ceará, Brasil. Revista de Geologia 29 (2), 263–271.

Albuquerque, M., Espinoza, J., Teixeira, P., De Oliveira, A., Corrêa, I., Calliari, L., 2013. Erosion or coastal variability: an evaluation of the DSAS and the change polygon methods for the determination of erosive processes on sandy beaches. J. Coast Res. 65 (10065), 1710–1714.

Al-Ruheili, A.M., Boluwade, A., 2021. Quantifying coastal shoreline erosion due to climatic extremes using remote-sensed estimates from Sentinel-2A data. Environmental Processes 8 (3), 1121–1140.

Alves, A.R., 2009. Long-term erosional hot spots in the southern Brazilian coast. J. Geophys. Res.: Oceans 114 (C2).

Anfuso, G., Bowman, D., Danese, C., Pranzini, E., 2016. Transect based analysis versus area based analysis to quantify shoreline displacement: spatial resolution issues. Environ. Monit. Assess. 188 (10), 1–14.

Anfuso, G., Domínguez, L., Gracia, F.J., 2007. Short and mid-term evolution of a coastal sector in Cadiz, SW Spain. Catena 70, 229–242.

Apostolopoulos, D.N., Avramidis, P., Nikolakopoulos, K.G., 2022. Estimating quantitative morphometric parameters and spatiotemporal evolution of the Prokopos Lagoon using remote sensing techniques. J. Mar. Sci. Eng. 10 (7), 931.

Apostolopoulos, N.D., Nikolakopoulos, G.K., 2020. Assessment and quantification of the accuracy of low-and high-resolution remote sensing data for shoreline monitoring. ISPRS Int. J. Geo-Inf. 9 (6), 391.

Araujo, R.S., Silva, G.V., Freitas, D., Klein, A.H.F., 2009. Georreferenciamento de fotografías aéreas e análise da variação da linha de costa. Métodos en teledetección aplicada a la prevención de riesgos naturales en el litoral 123–138.

Bacino, G.L., Dragani, W.C., Codignotto, J.O., Pescio, A.E., Farenga, M.O., 2020. Shoreline change retes along Samborombon Bay, Río de la Plata estuary, Argentina. Estuarine. Coastal and Shelf Science 237.

Barboza, E.G., Rosa, M.L.C., Dillenburg, S.R., Watanabe, D.S., Esteves, T., Martins, E.M., Gruber, N.L., 2018. Diachronic condition between maximum transgressive and maximum eustatic sea-level in Holocene: subsidies for coastal management. J. Coast Res. 85 (10085), 446–450.

Bértola, G., Sánchez-Caro, L., Garzo, P.A., 2021. Evolución del perfil de playa en zonas urbanas y periurbanas en el Partido de Villa Gesell, Buenos Aires, Argentina, para el período 1994-2021. Rev. Geogr. Chileerra Aust. 1, 41–54.

Bértola, G.R., 2006. Morfodinámica de playas del sudeste de la provincia de Buenos Aires (1983 a 2004). Lat. Am. J. Sedimentol. Basin Anal. 13 (1), 31–57.

Bértola, G.R., Farenga, M., Cortizo, L., Isla, F.I., 1999. Dinámica morfológica de las playas de Villa Gesell (1994-1996), provincia de Buenos Aires. Rev. Asoc. Geol. Argent. 54 (1), 23–35.

Bilmes, A., D'Elia, L., Lopez, L., Richiano, S., Varela, A., Alvarez, M.P., Bucher, J., Eymard, I., Muravchik, M., Franzese, J., Ariztegui, D., 2019. Digital outcrop modelling using "structure-from-motion" photogrammetry: acquisition strategies, validation and interpretations to different sedimentary environments. J. S. Am. Earth Sci. 96, 102325.

Bitencourt, V.J.B., Dillenburg, S.R., Manzolli, R.P., Barboza, E.G., 2020. Control factors in the evolution of Holocene coastal barriers in Southern Brazil. Geomorphology 360, 107180.

Blount, T.R., Carrosco, A.R., Cristina, S., Silvestri, S., 2022. Exploring open-source multispectral satellite remote sensing as a tool to map long-term evolution of salt marsh shorelines. Estuar. Coast Shelf Sci. 266.

Bose, M. de A., de Figueiredo, S.A., Calliari, L.J., Arigony-Neto, J., Goulart, E.S., Ferreira, J.A. de C., Albuquerque, M. da G., 2020. Os efeitos da elevação do nível do mar e do balanço sedimentar em um hotspot erosivo no litoral do Rio Grande do Sul, Brasil. Pesqui. em Geociencias 47 (2), e097101.

Busayo, E.T., Kalumba, A.M., 2021. Recommendations for linking climate change adaptation and disaster risk reduction in urban coastal zones: lessons from East London, South Africa. Ocean Coast Manag. 203, 105454.

Byun, D.S., Hart, D.E., 2019. On robust multi-year tidal prediction using T_TIDE. Ocean Sci. J. 54 (4), 657–671.

Cabezas-Rabadán, C., Pardo-Pascual, J.E., Almonacid-Caballer, J., Rodilla, M., 2019. Detecting problematic beach widths for the recreational function along the Gulf of Valencia (Spain) from Landsat 8 subpixel shorelines. Appl. Geogr. 110, 102047.

Carretero, S., Braga, F., Kruse, E., Tosi, L., 2014. Temporal analysis of the changes in the sand-dune barrier in the Buenos Aires Province, Argentina, and their relationship with the water resources. Appl. Geogr. 54, 169–181.

Carvalho, B.C., Dalbosco, A.L.P., Guerra, J.V., 2020. Shoreline position change and the relationship to annual and interannual meteo-oceanographic conditions in Southeastern Brazil. Estuarine. Coastal and Shelf Science 235, 1–10.

Cellone, F., Carol, E., Tosi, L., 2016. Coastal erosion and loss of wetlands in the middle Río de la Plata estuary (Argentina). Appl. Geogr. 76, 37–48.

Chrisben, S.C., Gurugnanam, B., 2022. Coastal transgression and regression from 1980 to 2020 and shoreline forecasting for 2030 and 2040, using DSAS along the southern coastal tip of Peninsular India. Geodesy and Geodynamics 13 (6), 585–594.

Clark, J.R., 1997. Coastal zone management for the new century. Ocean Coast Manag. 37 (2), 191–216.

Coca, O., Ricaurte-Villota, C., 2022. Regional patterns of coastal erosion and sedimentation derived from spatial autocorrelation analysis: pacific and Colombian caribbean. Coasts 2 (3), 125–151.

Coppin, P., Lambin, E., Jonckheere, I., Muys, B., 2002. Digital change detection methods in natural ecosystem monitoring: a review. Int. J. Rem. Sens. 25, 1565–1596.

Crowell, M., Leatherman, S.P., Buckley, M., 1993. Shore-line change rate analysis: long term versus short term data. Shore Beach 61 (2), 13–20.

D'Amico, G., Fucks, E., Carut, C., 2019. Dinamismo, complejidad y especificaciones de los litorales estuarinos: análisis de la dinámica litoral en Punta Atalaya, Buenos Aires, Argentina. Cuadernos de Investigación Geográfica 45 (2), 729–750.

De Oliveira, J.F., Barboza, E.G., Martins, E.M., Scarelli, F.M., 2019. Geomorphological and stratigraphic analysis applied to coastal management. J. S. Am. Earth Sci. 96, 102358.

Dillenburg, S.R., Barboza, E.G., Rosa, M.L.C., Caron, F., Bitencourt, V.J., 2020. Changes in the littoral drift system of the Uruguayan coast during the holocene and its influence in the continuing erosion in southern Brazil. J. Coast Res. 95 (SI), 453–457.

Dillenburg, S.R., Esteves, L.S., Tomazelli, L.J., 2004. A critical evaluation of coastal erosion in Rio Grande do Sul, Southern Brazil. An. Acad. Bras. Cienc. 76, 611–623.

Domínguez, L., Anfuso, G., Gracia, F.J., 2005. Vulnerability assessment of a retreating coast in SW Spain. Environ. Geol. 47 (8), 1037–1044.
El-Khalidi, K., Bourhili, A., Bagdanavičiūtė, I., Minoubi, A., Hakkou, M., Zourarah, B., Maanan, M., 2021. Coastal land use and shoreline evolution along the Nador lagoon Coast in Morocco. Geocarto Int. 1–17.
Enriquez-Acevedo, T., Botero, C.M., Cantero-Rodelo, R., Pertuz, A., Suarez, A., 2018. Willingness to pay for Beach Ecosystem Services: the case study of three Colombian beaches. Ocean Coast Manag. 161, 96–104.
Erkens, G., VAN Der Meulen, M.J., Middelkoop, H., 2016. Double trouble: subsidence and CO2 respiration due to 1,000 years of Dutch coastal peatlands cultivation. Hydrogeol. J. 24 (3), 551–568.
Esteves, L.S., 2004. Shoreline changes and coastal evolution as parameters to identify priority areas for management in Rio Grande do Sul, Brazil. Pesqui. em Geociencias 31 (2), 15–30.
Esteves, L.S., Toldo JR, E.E., Dillenburg, S.R., Tomazelli, L.J., 2002. Long-and short-term coastal erosion in Southern Brazil. J. Coast Res. (36), 273–282.
Fasano, J., Hernandez, M., Isla, F., Schnack, E., 1982. Aspectos evolutivos y ambientales de la laguna Mar Chiquita (provincia de Buenos Aires, Argentina). In.
Fenster, M.S., Dolan, R., 1993. Historical shoreline trends along the Outer Banks, North Carolina: processes and responses. J. Coast Res. 172–188.
Ferreira, T.A.B., Da Silva, A.G.A., Pérez, Y.A.R., Stattegger, K., Vital, H., 2021. Evaluation of decadal shoreline changes along the Parnaíba Delta (NE Brazil) using satellite images and statistical methods. Ocean Coast Manag. 202, 105513.
Fletcher, C., Rooney, J., Barbee, M., Lim, S.C., Richmond, B., 2003. Mapping shoreline change using digital orthophotogrammetry on Maui, Hawaii. J. Coast Res. 106–124.
Garzo, P.A., Dadon, J.R., Castro, L.N., 2019. Modelling environmental vulnerability of the biosphere reserve parque atlántico mar chiquito, Argentina, under agricultural and urban impacts. Ocean Coast Manag. 170, 72–79.
Gogoberidze, G., 2012. Tools for comprehensive estimate of coastal region marine economy potential and its use for coastal planning. J. Coast Conserv. 16 (3), 251–260.
Gracia, A., Rangel-Buitrago, N., Oakley, J.A., Williams, A.T., 2018. Use of ecosystems in coastal erosion management. Ocean Coast Manag. 156, 277–289.
Guimaraes Santos, C.A., Do Nascimento, T.V.M., Mishra, M., Da Silva, R.M., 2021. Analysis of long-and short-term shoreline change dynamics: a study case of João Pessoa city in Brazil. Sci. Total Environ. 769, 1–17.
Hansen, M.C., Loveland, T.R., 2012. A review of large area monitoring of land cover change using landsat data. Remote Sens. Environ. 122, 66–74.
Hanson, S., Nicholls, R., Ranger, N., Hallegatte, S., Corfee-Morlot, J., Herweijer, C., Andchateau, J., 2011. A global ranking of port cities with high exposure to climate extremes. Clim. Change 104, 89–111.
Hersbach, H., Bell, W., Berrisford, P., Horányi, A., Muñoz Sabater, J., Nicolas, J., Radu, R., Schepers, D., Simmons, A., Soci, C., Dee, D., 2019. Global Reanalysis: Goodbye ERA-Interim, Hello ERA5. ECMWF Newsletter. 159 ECMWF, Reading, United Kingdom, pp. 17–24.
Himmelstoss, E.A., Henderson, R.E., Kratzmann, M.G., Farris, A.S., 2018. Digital shoreline analysis system (DSAS) version 5.0 user guide. U.S. Geological Survey Open-File Report 1179, 110.
Isla, F.I., 1998. Holocene coastal evolution in Buenos Aires province, Argentina. In: Quaternary of South America and Antarctic Peninsula. Routledge, pp. 297–321.
Isla, F.I., Angulo, R.J., 2016. Tectonic processes along the South America coastline derived from Quaternary marine terraces. J. Coast Res. 32 (4), 840–852.
Isla, F.I., Cortizo, L.C., Schnack, E.J., 1996. Pleistocene and holocene beaches and estuaries along the southern barrier of Buenos Aires, Argentina. Quat. Sci. Rev. 15 (8–9), 833–841.
Isla, F.I., Bértola, G.R., Farenga, M.O., Serra, S.B., Cortizo, L.C., 1998. Villa Gesell: un desequilibrio sedimentario inducido por fijaciones de médanos. Revista de la Asociación Argentina de Sedimentología 5 (1), 41–51.
Isla, F.I., Cortizo, L., Merlotto, A., Bértola, G., Albisetti, M.P., Finocchietti, C., 2018. Erosion in Buenos Aires province: coastal-management policy revisited. Ocean Coast Manag. 156, 107–116.
Jana, A., Maiti, S., Biswas, A., 2016. Analysis of short-term shoreline oscillations along Midnapur-Balasore Coast, Bay of Bengal, India: a study based on geospatial technology. Modeling Earth Systems and Environment 2 (2), 1–10.
Juárez, V., Mantobani, J.M., 2006. La costa bonaerense: un territorio particular. In: Isla, F.I., Lasta, C.((Eds.), Manual de Manejo Costero para la Provincia de Buenos Aires. Mar del Plata. Editorial EUDEM, p. 41.
Komar, P.D., 1998. Beach Processes and Sedimentation, second ed. Prentice Hall, New Jersey, p. 544.
Kraus, N.C., Galgano, F.A., 2001. Beach erosional hot spot: types, causes, and solutions. In: Coastal Hydraulics Laboratory (CHL), Coastal and Hydraulics Engineering Technical.
Lanfredi, N.W., Pousa, J.L., Mazio, C.A., Dragani, W.C., 1992. Wave-power potential along the coast of the province of Buenos Aires, Argentina. Energy 17 (11), 997–1006.
Leatherman, S.P., Clow, J.B., 1983. UMD shoreline mapping project. IEE Geoscience and Remote Sensing Society Newsletter 22, 5–8.
Lemos, A.L.B., Sopchaki, C.H., 2020. Contribuição da ferramenta digital Shoreline Analysis System nos estudos de dinâmica costeira no estado do Ceará, Brasil. Rev. Equador 9 (3), 61–81.
Lu, D., Mausel, P., Brondizio, E., Moran, E., 2004. Change detection techniques. Int. J. Rem. Sens. 25 (12), 2365–2401.
Manno, G., Lo Re, C., Ciraolo, G., 2017. Uncertainties in shoreline position analysis: the role of run-up and tide in a gentle slope beach. Ocean Sci. 13 (5), 661–671.
Marcomini, S., López, R., Picca, P., Madanes, N., Bertolín, L., 2017. Natural coastal dune-field landforms, plant communities, and human intervention along Buenos Aires Northern Aeolian Barrier. J. Coast Res. 33 (5), 1051–1064.
Marcomini, S.C., López, R.A., 1997. Influencia de la urbanización en la dinámica costera, Villa Gesell, provincia de Buenos Aires, República Argentina. Revista de la Asociación Argentina de Sedimentología 4 (2), 79–96.
Martín Prieto, J.Á., Roig Munar, F.X., Rodríguez Perea, A., Pons Buades, G.X., Mir Gual, M., Gelabert Ferrer, B., 2018. Análisis de la evolución histórica de la línea de costa de la playa de es Trenc (S. de Mallorca): causas y consecuencias. GeoFocus 21, 187–214.
Martínez, C., Winckler Grez, P., Agredano Martín, R., Esparza Acuña, C., Torres, I., Contreras-López, M., 2022. Coastal erosion in sandy beaches along a tectonically active coast: the Chile study case. Prog. Phys. Geogr. 46 (2), 250–271. https://doi.org/10.1177/03091333211057194.
Mentaschi, L., Vousdoukas, M.I., Pekel, J.F., Voukouvalas, E., Feyen, L., 2018. Global long-term observations of coastal erosion and accretion. Sci. Rep. 8 (1), 1–11.
Mishra, M., Sudarsan, D., Kar, D., Naik, A.K., Das, P.P., Santos, C.A.G., Da Silva, R.M., 2020. The development and research trend of using dsas tool for shoreline change analysis: a scientometric analysis. J. Urban Environ. Eng. 14 (1), 69–77.
Moore, L.J., 2000. Shoreline mapping techniques. J. Coast Res. 16, 111–124.
Muehe, D., Klumb-Oliveira, L., 2014. Deslocamento da linha de costa versus mobilidade praial. Quat. Environ. Geosci. 5, 121–124.
Nassar, K., Mahmod, W.E., Fath, H., Masria, A., Nadaoka, K., Negm, A., 2018. Shoreline change detection using DSAS technique: case of North Sinai coast, Egypt. Mar. Georesour. Geotechnol. 37, 1–15.
Neumann, B., Vafeidis, A.T., Zimmermann, J., Nicholls, R.J., 2015. Future coastal population growth and exposure to sea-level rise and coastal flooding - a global assessment. PLoS One 10 (6).
Pajak, M.J., Leatherman, S., 2002. The high water line as shoreline indicator. J. Coast Res. 18 (2), 329–337. ISSN 0749-0208.
Pawlowicz, R., Beardsley, B., Lentz, S., 2002. Classical tidal harmonic analysis including error estimates in MATLAB using T_TIDE. Comput. Geosci. 28 (8), 929–937.
Phillips, M.R., Jones, A.L., 2006. Erosion and tourism infrastructure in the coastal zone: problems, consequences and management. Tourism Manag. 27 (3), 517–524.
Pianca, C., Holman, R., Siegle, E., 2015. Shoreline variability from days to decades: results of long-term video imaging. J. Geophys. Res.: Oceans 120 (3), 2159–2178.
Pivel, M.A.G., Speranski, N., Calliari, L.J., 2001. A erosão praial na costa Atlântica Uruguaia. Pesqui. em Geociencias 28 (2), 447–457.
Plant, N.G., Freilich, M.H., Holman, R.A., 2001. Role of morphologic feedback in surf zone sandbar response. Journal of geophysical research: Oceans 106 (C1), 973–989.
Poulter, B., Halpin, P.N., 2008. Raster modelling of coastal flooding from sea-level rise. Int. J. Geogr. Inf. Sci. 22 (2), 167–182.
Rahman, M.M., Bhattacharya, A.K., 2014. Saline water intrusion in coastal aquifer: a case study from Bangladesh. J. Eng. 4 (1), 7–13.
Rangel-Buitrago, N.G., Anfuso, G., Williams, A.T., 2015. Coastal erosion along the Caribbean coast of Colombia: magnitudes, causes and management. Ocean Coast Manag. 114, 129–144.
Romine, B.M., Fletcher, C.H., Frazer, L.N., Genz, A.S., Barbee, M.M., Lim, S.C., 2009. Historical shoreline change, southeast Oahu, Hawaii; applying polynomial models to calculate shoreline change rates. J. Coast Res. 25 (6), 1236–1253.
Różyński, G., 2005. Long-term shoreline response of a nontidal, barred coast. Coast. Eng. 52 (1), 79–91.
Ruggiero, P., Komar, P.D., Mcdougal, W.G., Marra, J.J., Beach, R.A., 2001. Wave runup, extreme water levels and the erosion of properties backing beaches. J. Coast Res. 17 (2), 407–419.
Santos, E.C., Bonetti, J., 2018. Análise da taxa de variação da linha de costa da Enseada de Tijucas (SC) em diferentees escalas temporais como indicadora de suscetibilidade costeira. Quat. Environ. Geosci. 9 (2), 19–25.
Scarelli, F.M., Barboza, E.G., Cantelli, L., Gabbianelli, G., 2016. Surface and subsurface data integration and geological modelling from the Little Ice Age to the present, in the Ravenna coastal plain, northwest Adriatic Sea (Emilia-Romagna, Italy). Catena 151, 1–15.
Scarelli, F.M., Cantelli, L., Barboza, E.G., Gabbianelli, G., 2017. Natural and anthropogenic influences on depositional architecture of the Ural Delta, Kazakhstan, northern Caspian Sea, during the past 70 years. Estuar. Coast Shelf Sci. 191, 10–20.
Schnack, E., Fasano, J., Isla, F.I., 1982. The evolution of mar chiquita lagoon coast, Buenos Aires province, Argentina. In: Proceedings International Symposium on Sea Level Changes in the Last 15.000 Years. magnitude and causes, South Carolina, pp. 143–155.
SHN, Servicio de Hidrografía Naval de la República Argentina, 2021. Online tide prevision service. Available at: http://www.hidro.gov.ar/oceanografia/tmareas/form_tmareas.asp. Available at:
Simões, R.S., Calliari, L.J., De Figueiredo, S.A., De Oliveira, U.R., De Almeida, L.P.M., 2022. Coastline dynamics in the extreme south of Brazil and their socio-environmental impacts. Ocean Coast Manag. 230, 106373.
Sowmya, K., Sri, M.D., Bhaskar, A.S., Jayappa, K.S., 2019. Long-term coastal erosion assessment along the coast of Karnataka, west coast of India. Int. J. Sediment Res. 34 (4), 335–344.
Spinosa, A., Ziemba, A., Saponieri, A., Damiani, L., El Serafy, G., 2021. Remote sensing-based automatic detection of shoreline position: a case study in apulia region. J. Mar. Sci. Eng. 9 (6), 57.
Stive, M.J., Aarninkhof, S.G., Hamm, L., Hanson, H., Larson, M., Wijnberg, K.M., Capobianco, M., 2002. Variability of shore and shoreline evolution. Coastal engineering 47 (2), 211–235.
Stockdon, H.F., Holman, R.A., Howd, P.A., Sallenger, A.H., 2006. Empirical parameterization of setup, swash, and runup. Coast. Eng. 53 (7), 573–588.

Timmermans, B.W., Gommenginger, C.P., Dodet, G., Bidlot, J.R., 2020. Global wave height trends and variability from new multimission satellite altimeter products, reanalyses, and wave buoys. Geophys. Res. Lett. 47 (9).

Turner, I.L., Harley, M.D., Short, A.D., Simmons, J.A., Bracs, M.A., Phillips, M.S., Splinter, K.D., 2016. A multi-decade dataset of monthly beach profile surveys and inshore wave forcing at Narrabeen, Australia. Sci. Data 3 (1), 1–13.

Turno-Orellano, H.A.T., Isla, F.I., 2004. Developing sinks for CO2 through forestation of temperate coastal barriers: an environmental business. Reg. Environ. Change 4 (1), 70–76.

Vallarino-Castillo, R., Negro Valdecantos, V., Moreno Blasco, L., 2022. Shoreline change analysis using historical multispectral landsat images of the pacific coast of Panama. J. Mar. Sci. Eng. 10 (12), 1801.

VAN Rijn, L.C., 2011. Coastal erosion and control. Ocean Coast Manag. 54 (12), 867–887.

Verón, M.J., Bértola, G.R., 2014. Aplicación del método de flujo de energía en el litoral de la provincia de Buenos Aires, Argentina. Lat. Am. J. Sedimentol. Basin Anal. 21 (1), 17–23.

Villate Daza, D.A., Sánchez Moreno, H., Portz, L., Portantiolo Manzolli, R., Bolívar-Anillo, H.J., Anfuso, G., 2020. Mangrove forests evolution and threats in the caribbean sea of Colombia. Water 12, 1113. https://doi.org/10.3390/w12041113.

Violante, R.A., 1992. Ambientes sedimentarios asociados a un sistema de barrera litoral del Holoceno en la llanura costera al sur de Villa Gesell, Provincia de Buenos Aires. Rev. Asoc. Geol. Argent. 47 (2), 201–214.

Virdis, S.G., Oggiano, G., Disperati, L., 2012. A geomatics approach to multitemporal shoreline analysis in Western Mediterranean: the case of Platamona-Maritza beach (Northwest Sardinia, Italy). J. Coast Res. 28 (3), 624–640.

Vos, K., Harley, M.D., Splinter, K.D., Simmons, J.A., Turner, I.L., 2019. Sub-annual to multi-decadal shoreline variability from publicly available satellite imagery. Coast. Eng. 150, 160–174.

Williams, A.T., Rangel-Buitrago, N., Pranzini, E., Anfuso, G., 2018. The management of coastal erosion. Ocean Coast Manag. 156, 4–20.

Wright, L.D., 1995. Morphodynamics of Inner Continental Shelves. CRC Press, Boca Raton.

Wright, L.D., Short, A.D., 1984. Morphodynamic variability of surf zones and beaches: a synthesis. Mar. Geol. 56, 93–118.

Zanchi watanabe, D.S., barboza, E.G., rosa, M.L.C., da, C., dillenburg, S.R., caron, F., do nascimento ritter, M., bitencourt, V.J.B.D.E., manzolli, R.P., 2023. Geomorfologia e padrões de empilhamento da barreira holocênica no Litoral Norte do Rio Grande do Sul. Revista Brasileira De Geomorfologia 24 (1).

Zhao, Q., Pan, J., Devlin, A.T., Tang, M., Yao, C., zamparelli, V., pepe, A., 2022. On the exploitation of remote sensing technologies for the monitoring of coastal and river Delta regions. Rem. Sens. 14 (10), 2384.

J. Geogr. Sci. 2025, 35(1): 206-230
DOI: https://doi.org/10.1007/s11442-025-2319-2

Touristic urbanization and greening of coastal dune fields:
A long-term assessment of a temperate sandy barrier of Argentina

GARZO Pedro Andrés[1,2], DADON José Roberto[3,4], ISLA Federico Ignacio[1,2]

1. Instituto de Investigaciones Marinas y Costeras (IIMyC -CONICET/UNMDP), Av. Juan B. Justo 2550, Mar del Plata, 7600, Buenos Aires, Argentina;
2. Instituto de Geología de Costas y del Cuaternario Dr. Enrique J. Schnack (IGCC - CIC/UNMDP), Funes 3350, Mar del Plata, 7600, Buenos Aires, Argentina;
3. Universidad de Buenos Aires, Facultad de Arquitectura, Diseño y Urbanismo, Centro de Investigaciones Gestión de Espacios Costeros (GEC - FADU / UBA), Intendente Güiraldes 2160, Pabellón III, Piso 4, Ciudad Autónoma de Buenos Aires, 1428, Argentina;
4. Consejo Nacional de Investigaciones Científicas y Técnicas (CONICET), Argentina

Abstract: Dune barrier systems represent highly sought-after coastal landscapes for tourism and urban development around the world. However, a century ago, they were considered hazardous environments due to their great dynamic nature. As a result, stabilization practices were considered necessary. The systematic introduction of fast-growing exotic trees helped stabilize the sand, making it easier for tourism urbanization to take place, but also leading to erosion processes. This paper aims to assess long-term changes in vegetation cover over a large temperate barrier in Argentina. This complex region includes urban resorts, afforestation zones, and protected areas. A GIS-based geospatial analysis was conducted using a large satellite database (> 350 images), and the future evolution of the vegetation was modeled. The results revealed two primary spatiotemporal patterns associated with a gradual expansion of vegetation cover, accompanied by a concurrent reduction in sandy areas. In 1986, the dune area comprised 75% more surface than vegetation, whereas in 2021, it represented 60% less than vegetation. Furthermore, the 2050 scenario suggests a potential 40% reduction of dunes in certain areas. It is necessary to enhance management actions aimed at maintaining dune mobility and ensuring local and regional sediment balance. Long-term management strategies must focus on restoring native plant communities and controlling invasive species, and avoiding new dune fixation initiatives based on the introduction of exotic species.

Keywords: nature reserves; afforestation; sediment balance; dune management; NDVI

Received: 2024-02-03 **Accepted:** 2024-08-05

Foundation: Ministry of Science, Technology and Innovation of Argentina (Impact.AR N° 106-RESOL-2022-224-APN-SACT#MCT); Nacional Council of Scientific and Technical Research–CONICET–(PIP 21/23 1122020010-0041CO - RESOL-2021-1639-APN-DIR#CONICET)

Author: Pedro A Garzo, PhD, E-mail: pgarzo@agro.uba.ar

1 Introduction

Coastal areas are crucial environments for socio-economic development and human well-being on a global scale. Currently, more than 40% of the Earth's population lives within 100 km of a coast (Busayo and Kalumba, 2021), and projections point to an increase in population density in these areas by approximately a quarter by 2050 (Zhao *et al*., 2022). In particular, dune barrier systems, which encompass approximately 15% of the world's coasts (Pilkey *et al*., 2009), provide essential ecosystem goods and services related to physical and ecological protection. These services include flood control, sediment stabilization, wave attenuation, storm protection, nutrient recycling, salt intrusion control, and freshwater storage and replenishment (Gómez-Pina *et al*., 2002). These fragile and dynamic environments are primarily controlled by three major driving forces: wind patterns, sand availability, and vegetation cover (Hesp *et al*., 2010). Therefore, climate conditions play a significant role in the formation, stabilization, and evolution of dunes (Muhs and Maat, 1993).

Dune barrier systems are currently among the most demanded landscapes for sea-and-sun tourism and recreational uses, supporting many coastal economies worldwide (Schlacher *et al*., 2008). As one of the main drivers of coastal development (Da Silva and Schwingel, 2019), tourism leads to several land use and land cover (LULC) changes, and constitutes a major anthropogenic impact on coastal areas worldwide (Clark, 1997). In particular, coastal urbanization and dune afforestation are the most relevant LULC changes related to tourism development (Okello *et al*., 2015).

Just a century ago, dunes were regarded as hazardous and fragile landforms that threatened human development. In order to stabilize the sandy substrate of dunes, the systematic implantation of rapid-growth trees, often including exotic species has been the preferred management strategy (Doody, 2005). This approach has facilitated subsequent urban expansion onto these environments (Castillo and Moreno-Casasola, 1996). However, this short-term stabilization can lead to the fragmentation of the original dune landscape, resulting in several environmental impacts and threatening long-term environmental sustainability (Feagin *et al*., 2010). The replacement of native vegetation by exotic species, alterations in plant assemblages, changes in species richness and diversity, modifications in phytosociological distribution, shifts in total vegetation cover, and environmental fragmentation account for some of these impacts (Pauchard *et al*., 2006; Calderisi *et al*., 2021; Pintó *et al*., 2023).

Regarding abiotic conditions, sedimentary imbalance appears as the primary impact of dune fixation, as vegetation can drastically alter geomorphological processes by modifying the aeolian dynamics (Anthonsenet *et al*., 1996). The stabilization of bare dune areas restricts the natural cycle of sediment exchange between them, the beach and the surf zone (Avis, 1989). Therefore, afforestation practices can promote coastal erosion processes due to a reduction in sand availability and an alteration in the erosion/deposition balance (Provoost *et al*., 2011). These impacts have been widely recognized for sandy barriers worldwide (Illenberger, 1993; Isla *et al*., 1998; Ratas *et al*., 2008; Palma *et al*., 2011; Luo *et al*., 2015; Pranzini, 2018). Many countries have recognized the negative effects of afforestation costal environments and have enacted regulations to prevent or control the practice (DEFRA, 2007).

The economy of tourism-based coastal villages is directly related to urban development, and they rely on the preservation of their landscapes and the bathing quality of their beaches (Klein and Osleeb, 2010). Coastal tourism creates various environmental impacts but is also

vulnerable to these changes (Li *et al*., 2016). To protect biodiversity, landscape structure, and geomorphological features of barrier systems, as well as to preserve these unique and complex environments, several coastal protected areas have been established as a management and conservation strategy (Stoms *et al*., 2005). In addition, the control of dune plant communities, whether native or exotic, has been recognized as a crucial aspect of dune management in recent decades (Vranjic *et al*., 2012).

Remote sensing data and Geographic Information Systems (GIS) have been widely used for monitoring geospatial processes. In particular, vegetation monitoring has been extensively carried out by using the Normalized Difference Vegetation Index (NDVI). This spectral index is directly linked to biophysical variables such as leaf area, productivity, biomass, and canopy coverage (Weiss *et al*., 2004). In addition, its mathematical simplicity makes it a valuable tool for analyzing large temporal series across different multispectral remote sensing data (Gu *et al*., 2009).

Texeira-Pinto and Reis-Fernandes (2011) conducted an NDVI-based evaluation of vegetation cover evolution in dune environments along the northeastern Brazilian coast over 21 years (1986–2007) using a series of four satellite images. Cortizo and Isla (2012) employed a similar approach to assess a dune barrier system in southern Buenos Aires, Argentina. In addition, Goñi *et al*. (2016) and Bustos *et al*. (2016) estimated the NDVI temporal variation for small coastal villages of the Buenos Aires province. These studies relied on small sets of satellite images. However, in recent years, the Google Earth Engine (GEE; https:// earthengine.google.com/) platform has evolved into a high-performance tool for processing large geospatial databases within a cloud-based system, enhancing the analysis of extensive time-series datasets (Gorelick *et al*., 2017). Moreover, this platform has recently been used in coastal studies (Chen *et al*., 2021; Fitton *et al*., 2021).

The main objective of this paper was to assess long-term vegetation cover changes over a complex dune barrier system located in Buenos Aires, Argentina. This barrier system has been subjected to tourism urbanization, afforestation initiatives, recreational activities, and even conservation management strategies and protected areas. This barrier and its beaches hold significant local importance as they constitute the primary resource of an exclusively tourism-based economy. A geospatial analysis, based on the spectral assessment of a large satellite database processed using the GEE platform was conducted between the years 1986 and 2021. NDVI and GIS-based techniques were used to determine vegetation cover changes over time as an indicator of dune degradation. A predictive model was proposed to estimate the mid-term future evolution of the barrier vegetation coverage. The results of this study will be useful for the proper management of urban beaches and dune-protected areas.

1.1 The Eastern Sandy Barrier and study area

The Eastern Sandy Barrier, situated in the northernmost sector of the Atlantic coast of the Buenos Aires province, Argentina, evolved in relation to the mid-Holocene sea-level fluctuation as did the great majority of barriers and spits of the South American coast. This fluctuation resulted in the burial of an extensive plain that included coastal lagoons and marshes of the Salado River basin, under a dune field that currently extends along 200 linear km of coastline and reaches widths up to 3 km (Isla, 1998). The study area of this work is represented by the southernmost sector of this barrier, comprising 60 km of non-interrupted linear

shoreline extension and covering an area of 13,350 ha of sand barrier landscapes (Figure 1). In this sector, the barrier narrows gradually from north to south, ultimately reaching its end point at the sea outlet of the Mar Chiquita coastal lagoon.

This area of interest (AOI) is characterized by a complex array of land uses, land ownership, jurisdictional limits, and conservation states. Its northern sector, corresponding to Villa Gesell County, encompasses three coastal tourist villages (Mar de Las Pampas, Las Gaviotas, and Mar Azul; hereafter referred to as northern villages, NV) covering an area of 690 ha. It also includes the Faro Querandí Nature Reserve (FQ), spanning 4280 ha. In the southern sector, located in Mar Chiquita County, the Mar Chiquita Nature Reserve (MC) represents an area of 4380 ha over the dune barrier system. Moreover, there are diverse private estates situated between the northern villages and the FQ reserve, as well as between reserves, encompassing 2100 ha and 1900 ha, respectively (hereafter referred to as northern villages' private lands, PL-NV, and intra-reserves' private lands, respectively, PL_IR).

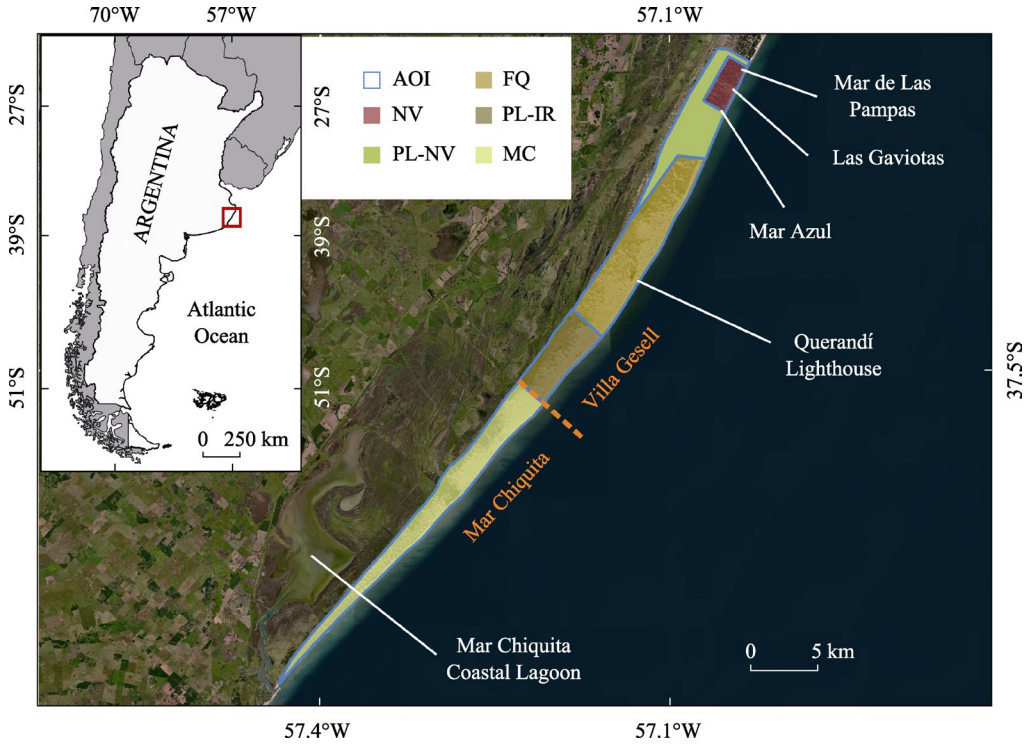

Figure 1 Location of the study area, in the southernmost sector of the Eastern Barrier of Buenos Aires province, Argentina. References: area of interest (AOI); northern villages (NV); northern villages' private lands (PL-NV); Faro Querandí Nature Reserve (FQ); intra-reserves' private lands (PL-IR); Mar Chiquita Nature Reserve (MC). The Orange dotted line represents the limit between Villa Gesell and Mar Chiquita counties.

In this coastal sector, the littoral drift provides a continuous sand supply representing a potential net balance between 400,000 and 700,000 m^3/yr. in the S-N direction (Framiñan, 1990). Both southern and northern winds are frequent. However, southern winds are the most intense and are associated with extreme weather events (Lanfredi *et al.*, 1992). Dunes are mainly composed of mid-grain sands, and they exhibit various morphologies, including transverse, parabolic, and barchanoid (Isla *et al.*, 1998). These coastal landforms host coastal

aquifers, characterized by a lenticular-shaped water table, which serve as the main hydrological resource for human development as well as for afforestation purposes.

1.2 Tourism development and conservation responses

During the second half of the 20th century, the Eastern Sandy Barrier experienced exponential growth in sea and sun tourism. By the mid-1970s, the city of Villa Gesell reached the highest urbanization rates in Argentina (Juárez and Isla, 1999). Today, it attracts over 2.1 million visitors during the summer season (Source: Tourism Office of Villa Gesell). The surge in tourism development was accompanied by a systematic replacement of active dunes with urban covers and rapid-growth exotic forests for dune fixation (Isla, 2013).

As described by Cabrera (1941), before the advent of massive tourism, the vegetation on this barrier was characterized as an open grassland composed of about 70 species. It was dominated by the *Panicum spp.*, with psammophilous species adapted to sand burial and saltwater conditions (Faggi and Dadon, 2011). The plant coverage was characterized by 80% species richness of perennial grasses and 20% of low shrubs. Native trees were absent in this barrier. Moving westwards, the vegetation grades to larger herbaceous and shrub assemblages of the Pampean lowlands' environments, characterized by hygrophilous and fogger species (Celsi, 2016). The tree species used for dune stabilization purposes were exotic, with *Pinus pinaster*, *Pinus radiata*, *Tamarix ramosissima*, *Cupressus lambertiana*, and *Acacia longifolia* being the most representative. In addition, domestic gardening and green areas' stewardship have also been an important source of exotic species introduction (Faggi and Dadon, 2010). The systematic replacement of dune areas and native vegetation by afforestation and gardening species has led to a decrease in sand availability in the Eastern Sandy Barrier (Marcomini *et al*., 2017). Moreover, this alteration of the original landscape morphology and sedimentary balance has induced coastal erosion problems (Isla *et al*., 1998). The environmental impacts have led to the creation of two important dune reserves, with the primary objective of conserving the regional sedimentary balance and ensuring hydrological sustainability through the replenishment of coastal aquifers.

The Faro Querandí Nature Reserve (FQ), managed under local jurisdiction, is located in the southernmost sector of Villa Gesell County. Established in 1996, it spans approximately 20 km of linear shoreline and is categorized as a "multiple-use reserve", allowing for recreational, touristic, and research activities within its boundaries. In addition, it includes 60 ha of exotic afforestation lands, owned by the Argentine Army and corresponding to the Querandí Lighthouse (Celsi *et al*., 2016; Figure 1). The Mar Chiquita Nature Reserve (MC), created as an UNESCO World Biosphere Reserve in 1996 and managed under local jurisdiction, encompasses the Mar Chiquita Coastal Lagoon, the only microtidal lagoon in Argentina. Over time, various conservation statuses were assigned, resulting in an overlap of management actions and protection strategies. It holds designations such as local reserve, national defense nature reserve, wildlife refuge, BirdLife International Area, and dune reserve. The latter was established in 2009 under the administration of the Buenos Aires province, covering exclusively 30 km of linear shoreline and dune landscapes in the terminal sector of the barrier (Garzo *et al*., 2019). Both reserves (FQ and MC) are bordered on the west by private rural estates corresponding to the Pampean region.

2 Materials and methods

2.1 Method workflow

To assess the vegetation cover changes between 1986 and 2021, four main methodological steps were conducted: satellite data retrieval (a), pre-processing and NDVI estimation (b), land cover categorization (c), and vegetation cover change assessment and forecasting (d) (Figure 2).

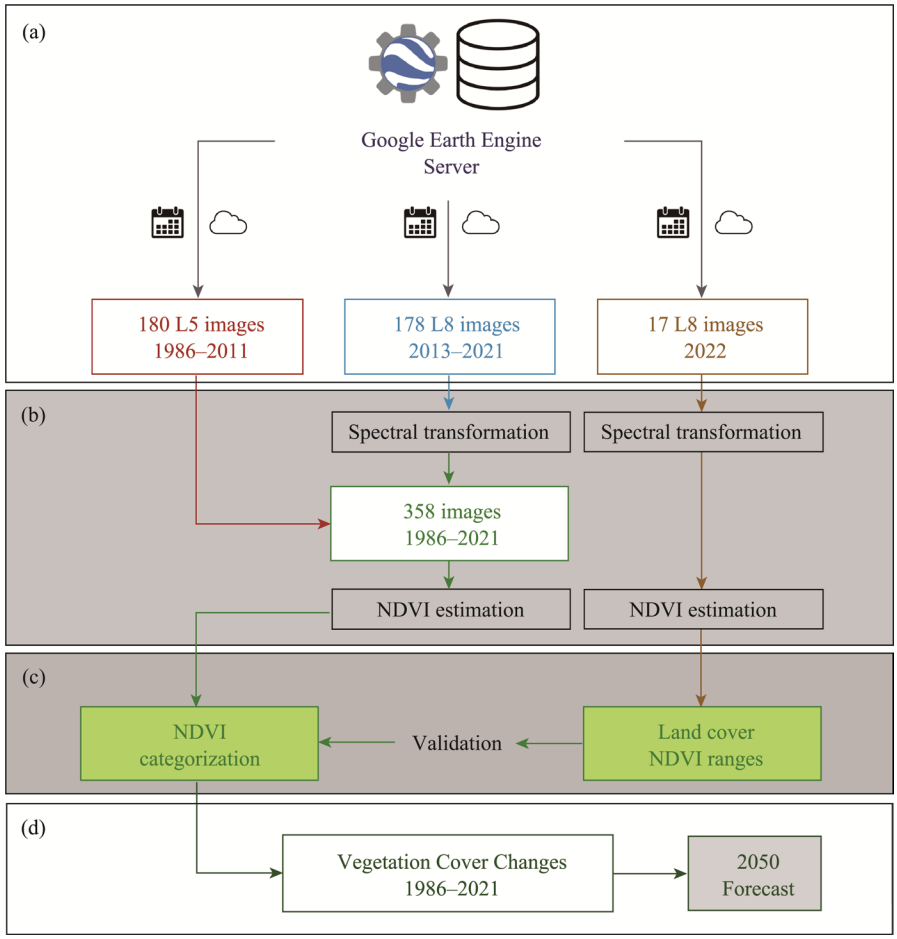

Figure 2 Schematic flowchart considering the main steps of this work (a. satellite data retrieval; b. pre-processing and NDVI estimation; c. land cover categorization; d. vegetation cover change assessment and forecasting)

2.2 Satellite data

Optical data were retrieved from the GEE catalog (https://developers.google.com/earth-engine/datasets/catalog/landsat) and consisted of all the available imagery from the USGS Landsat 5 TM (L5) and Landsat 8 OLI (L8) sensors covering the 1986–2021 period. For both sensors, top-of-atmosphere (TOA) reflectance data with 30 m spatial resolution and less than 10% of pixel-scale mean cloud coverage in the AOI was considered, resulting in 358 images (180 from L5 and 178 from L8; Table 1).

Table 1 Detail of satellite data used for this study. Dates are in MM/DD/YYYY format.

Characteristic		L5	L8
Sensor		Landsat 5 TM	Landsat 8 OLI
Processing level		Collection 2 Tier 1	Collection 2 Tier 1
Data type		TOA reflectance	TOA reflectance
Number of images		180	178
Mean pixel cloud cover (%)		1.38	1.67
Date	From	01/06/1986	04/22/2013
	To	08/30/2011	12/24/2021
Spatial resolution (m)		30	30
Path/Row		223/86 and 224/86	223/86 and 224/86

An additional dataset of 17 scenes from L8 images from 2022 was also included. These images were only taken into account for the calibration and validation steps, while they were ruled out for the spectral analysis of the data. The data retrieval was conducted using the open access and free tools provided by the GEE Code Editor Platform (https://code. earthengine. google.com/).

2.3 Data pre-processing and NDVI estimation

Before conducting the NDVI assessment steps, the spectral transformation method developed by Roy *et al*. (2016) was applied to estimate comparable results between L5 and L8 images. This method enables the spectral transformation of reflectance data, taking into account differences in radiometric resolution among sensors which can lead to inconsistencies when comparing multi-platform time series satellite data. As a consequence, the red and near-infrared bands of L8 data (band 4 and band 5, respectively) were subjected to a set of statistical transformation functions to obtain reflectance data comparable to those of the corresponding bands in L5 data (Figure 2). Subsequently, NDVI was estimated at a pixel scale for the entire dataset following:

$$NDVI = (IR - R) / (IR + R)$$

where R and IR represent the red and infrared TOA reflectance values, respectively. This index takes values ranging from –1 to 1, with positive values indicating green vegetated surfaces. The geospatial data pre-processing and processing steps were also conducted using the GEE Code Editor Platform tools.

2.4 NDVI categorization and vegetation cover change (1986–2021)

To assess temporal changes in vegetation cover, a pixel categorization was performed by using the open-source QGIS software (V. 3.8.2 - https://qgis.org/es/site/; QGIS, 2022). To calibrate the procedure, ground control sites (GCSs) with known land cover were identified. These GCSs were georeferenced by GPS/GNSS mark points retrieved from 2022 field surveys, corresponding to four land cover classes (LCCs): (1) bare dune areas (D); (2) herbaceous dune vegetation (H); (3) Pampean lowlands' vegetation (P); and (4) urban settlements vegetation (U). The latter was represented by exotic rapid-growth afforestation for dune fixation and ornamental species used for gardening purposes. Each LCC was characterized us-

ing 3 GCSs, representing a total of 12 control sites. Mean annual NDVI and standard deviation values were calculated for each GCS by using 12 L8 images (one image per month) from 2022, resulting in characteristic NDVI ranges for each LCC. In addition, mean seasonal NDVI and standard deviation values were assessed to compare the intra-annual variability and to determine the existence of statistical significance between seasonal estimations.

A validation step was conducted using the remaining 5 L8 images from 2022. For this purpose, an accuracy assessment was performed with the SCP Plugin Tool for QGIS software (Congedo, 2021), taking into account 2 GCSs for each LCC, and resulting in an overall accuracy of 88.3%. Table 2 presents the characteristic NDVI ranges for each LCC.

Table 2 Minimum, maximum, mean value, and standard deviation (Std) of characteristic NDVI ranges for the land cover classes estimated during the calibration procedure with L8 images from 2022

Land cover type	Land cover class	Min value	Max value	Mean value	Std
Non-vegetation	Bare dune areas (D)	0.013	0.112	0.063	0.002
Vegetation	Herbaceous (H)	0.153	0.329	0.261	0.018
Vegetation	Pampean lowlands (P)	0.351	0.433	0.392	0.027
Vegetation	Urban settlements (U)	0.454	0.647	0.550	0.036

Subsequently, the mean annual NDVI was estimated for the 1986–2021 period using the 358 available images. Each of these mean NDVI maps was categorized based on the characteristic NDVI ranges. Pixels that did not fall within the defined ranges were excluded from the assessment. Data processing was conducted using the QGIS software and various Python libraries (http://www.python.org; Python, 2023). The statistical analysis of NDVI estimations and the paired t-test for assessing intra-annual variability significance, assuming normality of differences between seasonal samples, were performed using the InfoStat v2020 Software (Di Rienzo *et al*., 2020; https://www.infostat.com.ar/).

2.5 Vegetation cover forecast (2050)

To predict vegetation cover changes through 2050, the Modules for Land-Use Change Simulation (MOLUSCE) Plugin tool for QGIS software was used (http://hub.qgis.org/ projects/molusce). Based on the LCC changes for the 1986–2003 period, a transition potential modeling was conducted following an Artificial Neural Network (ANN) approach. LCC was considered as the spatial dependent variable while the Argentinian Digital Elevation Model represented the independent variable (MDE-Ar V2.1 30 m × 30 m IGN; https://www.ign.gob.ar/NuestrasActividades/Geodesia/ModeloDigitalElevaciones/Mapa). Following the parameters used in Muhammad *et al*. (2022), the ANN learning process included 5,000 random samples and 100 iterations over a neighborhood value of 1x1 pixels with a learning rate of 0.001. The resulting model enabled us to predict the 2004–2021 LCC changes. Subsequently, the simulated 2021 LCC scenario was validated through a prediction accuracy assessment based on a kappa validation and using the 2021 LCC image estimated from optical data as a reference map. Once the model was satisfactorily trained and validated, LCC optical data maps from 1986 and 2021 were used as inputs following the same ANN approach, generating a 2050 LCC map prediction.

3 Results

3.1 NDVI assessment

The statistical analysis of the 2022 set of L8 images, conducted during the calibration procedure, revealed that the mean seasonal NDVI values did not exhibit statistically significant differences among them. The paired t-test for dependent samples was performed for the seasonal means of the different land cover classes. The p-value for bilateral estimation at a significance level of 5% ranged between 0.1217 (summer-winter for urban settlements' vegetation) and 0.9340 (summer-spring for bare dune areas). These results did not allow for the rejection of the equality hypothesis between seasonal means for any of the season-cover combinations. Moreover, differences of zero between seasonal means were included in the 95% confidence interval during this statistical analysis.

In addition, 2020 was taken as a pilot case as it represented the year with the highest number of satellite acquisitions (21) distributed throughout the temporal series dataset. Variations between maximum and minimum NDVI values were calculated at 0.03 (D), 0.05 (U), 0.09 (H), and 0.11 (P), with the lowest values occurring at the end of the winter season (Figure 3).

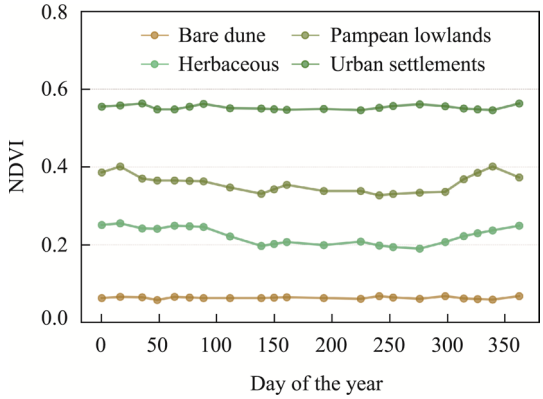

Figure 3 Temporal variation of NDVI values for each land cover class during 2020

The five zones considered exhibited a consistent and gradual increase in the annual average NDVI for the 1986–2021 period (Figure 4a). FQ and MC, showed rates of NDVI increase of 1.4%/yr (R^2 = 0.95; p<0.05) and 1.7%/yr (R^2 = 0.89; p<0.05) respectively. The PL-NV zone presented NDVI values ranging from 0.249 to 0.351, with a 1.6%/yr increase (R^2 = 0.72; p<0.05). Finally, the NV zone had the highest NDVI values, starting at 0.371 in 1986 and reaching 0.432 in 2021. However, its growth rate was estimated as only 0.8%/yr (R^2 = 0.67; p<0.05), surpassing only the 0.7%/yr increase (R^2 = 0.94; p<0.05) observed in PL-IR.

The NDVI change between 1986 and 2021 revealed that ~37% of the AOI surface experienced an increase greater than 0.1 in its values, while ~57% did not show significant changes throughout the tested period (–0.1≤NDVI change≥0.1) (Figure 4b). Additionally, ~6% exhibited an NDVI decrease (< –0.1) by 2021. The ~32% and ~36% of MC and FQ reserve areas presented NDVI increases, respectively. In addition, PL-NV and NV zones

exhibited that ~46% and ~42% of their surface were subjected to an NDVI increase, respectively. At the same time, ~12% of the Mar Chiquita reserve surface represented a decrease in the estimated values.

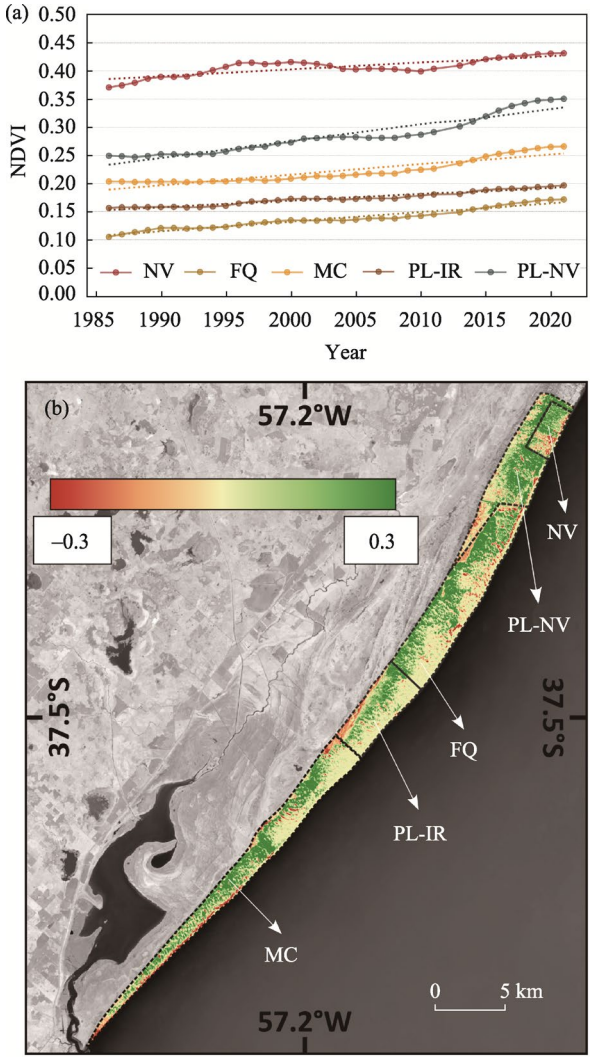

Figure 4 Annual average NDVI change for the studied period (a), Dotted lines represent the linear regression fitting curves; NDVI difference between 2021 and 1986 for the study area (b)

3.2 Vegetation cover changes (1986–2021)

The assessment of LCC characteristic ranges presented in table 2 led to the categorization of the 36 years of annual mean NDVI images for each zone. The northern villages' zone showed relative decreases of 3.3% and 19.7% in dune (23 ha) and herbaceous (136 ha) areas, respectively, between 1986 and 2021 (Figure 5a). In contrast, pampean lowlands and urban covers presented 3.1% (21 ha) and 20.1% (138 ha) relative increases, respectively. The PL-NV zone, representing the spatial transition between urban areas and the Faro Querandí

Nature Reserve, exhibited a similar pattern. D and H areas decreased by 17.6% (370 ha) and 6.7% (141 ha), respectively, while P and U cover increased by 14.2% (297 ha) and 11.5% (241 ha), respectively (Figure 5b).

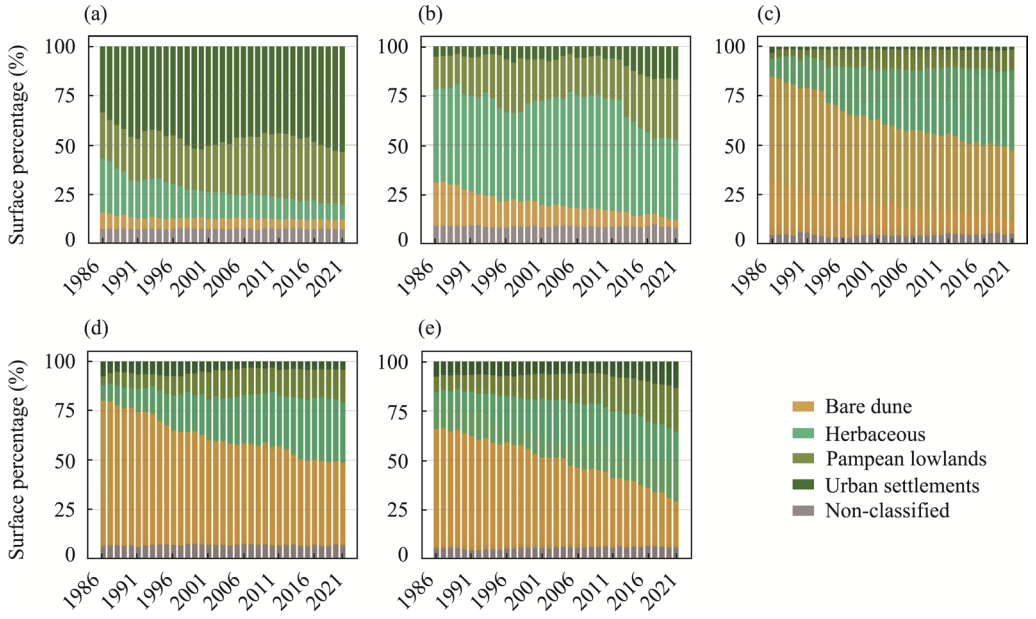

Figure 5 Surface percentage variation of LCCs (1986–2021) for northern villages (a); northern villages' private lands (b); Faro Querandí Nature Reserve (c); intra-reserves' private lands (d); Mar Chiquita Nature Reserve (e)

The FQ, PL-IR, and MC zones exhibited relative decreases in dune surfaces of 38.1% (1628 ha), 31.5% (598 ha), and 37.1% (1626 ha), respectively. In the case of FQ and PL-IR, H and P covers increased while urban vegetation areas decreased (Figures 5c and 5d). In FQ, H and P increased by 31.6% (1350 ha) and 7.6% (323 ha), respectively, while in PL-IR they increased by 22.1% (426 ha) and 12.0% (228 ha), respectively. However, U vegetation in both areas decreased by 1.5% (64 ha) and 3.3% (63 ha), respectively. In contrast, for the MC zone, all three vegetation classes (H, P, and U) showed increases of 16.8% (737 ha), 14.3% (626 ha), and 5.6% (246 ha), respectively (Figure 5e). Across all five zones, non-classified pixels ranged between 4% and 8%.

3.3 Vegetation cover forecast (2021–2050)

The 2021 predicted scenario was validated against optical data obtaining an overall percentage of accuracy of 86.41% (Overall Kappa Value = 0.85). This training procedure made it possible to generate the 2050 LCCs forecast based on the 1986–2021 data (Figure 6). For NV, PL-NV, and MC zones, the predicted scenario showed relative losses of 0.2% (1 ha), 2.3% (18 ha) and 0.1% (2 ha) in D area, respectively. For NV, a replacement of 18 ha of H by 12 ha and 6 ha of P and U, respectively, was estimated. In contrast, for PL-NV, a 23 ha and 47 ha reduction of H and P vegetation were accompanied by an increase of 101 ha in urban covers. MC followed this pattern, with 100-ha and 57-ha decreases in herbaceous and

pampean vegetation at the expense of a 153-ha increase in U covers. In contrast, FQ and PL-IR zones showed consistent decreases in the D area of 17.9% (767 ha) and 15.5% (295 ha), respectively. In both cases, these reductions are linked to an increase in the surface of H (155 ha and 139 ha, respectively), P (903 ha and 133 ha, respectively) and U (12 ha and 10 ha, respectively) covers.

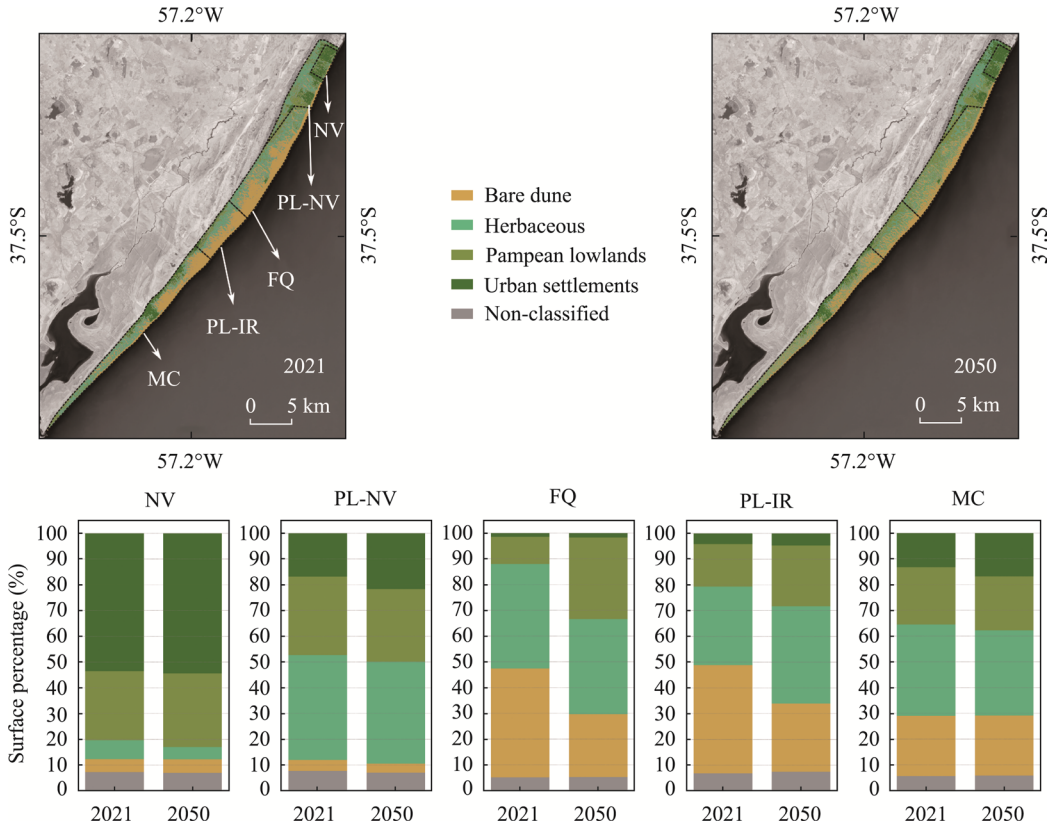

Figure 6 Spatial distribution of LCCs in 2021 and 2050-forecasted scenario (Up); LCCs surface percentage (2021 and 2050) (Down) for the AOI

4 Discussion

Previous satellite-based NDVI estimations for vegetation cover assessment have been conducted for the dune fields of the Buenos Aires province (Cortizo and Isla, 2012; Bustos *et al.*, 2016; Goñi *et al.*, 2016). Other authors have assessed this index and its correlation with biophysical parameters in coastal marshes of the same region through field surveys (Gonzáles Trilla *et al.*, 2013 and 2016). Moreover, previous floristic and coverage censuses have been carried out for the study area (Cabrera, 1941; Faggi and Dadon, 2010; Faggi and Dadon, 2011; Marcomini *et al.*, 2017). The novelty of this paper lies in presenting the first regional NDVI long-term analysis for the southernmost sector of the Eastern Sandy Barrier, based on the spectral assessment of a large satellite database (> 350 images). It also considers the country's most important coastal dune reserves as part of a complex single barrier system, rather than as isolated entities. For this purpose, Google Earth Engine was used to compute a

large amount of geospatial data, representing the first application of this platform for vegetation assessment in the coastal dune fields of the Buenos Aires province.

This methodological approach, calibrated and validated against georeferenced field data information, reflected an accuracy of over 85%. These results are consistent with recent elsewhere NDVI assessments (Thomas *et al*., 2021), as well as coastal LULC classifications (Vijay *et al*., 2020). The accuracy loss and the low NDVI values could be attributed to the surface heterogeneity and sparse vegetation, considering the relationship between vegetation patches and the spatial resolution of Landsat imagery (30 m × 30 m).

The intra-annual variability analysis did not exhibit statistically significant differences among mean seasonal NDVI values for the different land cover classes. In addition, urban vegetation exhibited the highest NDVI values, followed by P, H, and D, respectively (Figure 3). Greater NDVI values of forests over shrublands and grasslands were assessed (Ghebrezgabher *et al*., 2020). Seasonal differences ranged from 0.11 (P) to 0.03 (D). These findings contrast with those related to deciduous forests (Wang *et al*., 2005), crop fields (Huang *et al*., 2014), or even annual vegetation such as coastal grasslands (Trepekli *et al*., 2016), where NDVI differences can exceed ~0.40.

In contrast, our data showed a small intra-annual variability with the highest NDVI peaks occurring in early summer and the lowest in late winter, a seasonal pattern consistent with previous studies for the Pampean Region (Baeza and Paruelo, 2020). In addition, Marcomini *et al*. (2017) identified minor annual changes in plant phenology and growth rates for the vegetation of this barrier. Therefore, the results suggest that intra-annual variability may be negligible when estimating the mean annual NDVI time series for vegetation change assessment of the study zone. However, slight differences can be identified in strong El Niño-Southern Oscillation (ENSO) periods as 1997–1998 and 2015–2016 (Figure 4a).

The five zones exhibited a generalized and constant increase in their mean annual NDVI estimates between 1986 and 2021 (Figure 4a), a trend that had already been assessed for South America at a regional scale (Paruelo *et al*., 2004). Fairbanks and McGwire. (2004) indicated that persistent increments in green vegetation between locations represent greater differences than phenological variations. Thus, interpixel variability seems to be more representative than intrapixel variability. Being consistent with the results of this study, NDVI-increasing time series tend to reflect smoothly progressive patterns of vegetation growth beyond their seasonal variability (Doughty *et al*., 2021).

A particular pattern was observed in the southernmost sector of the MC zone, where ~500 ha exhibited a decrease in NDVI values over the studied period (Figure 4b). In this area, private estates' owners used to fire the marshy areas as a management practice to prevent invasive cyperaceous plants to become shrubs. At the same time, psammophilous assemblages of *Spartina ciliate* and *Panicum racemosum* served as pioneers on the mobile substrate of primary dunes (Celsi, 2016). These species colonize the upper sections between the backshore and the foredune foot, representing the initial plant cover in a beach-dune direction (Marcomini *et al*., 2017). The observed NDVI decrease pattern is representative of those coastal dune areas under erosion processes where the shoreline retreat displaces the establishment of pioneer species landwards (Figure 7).

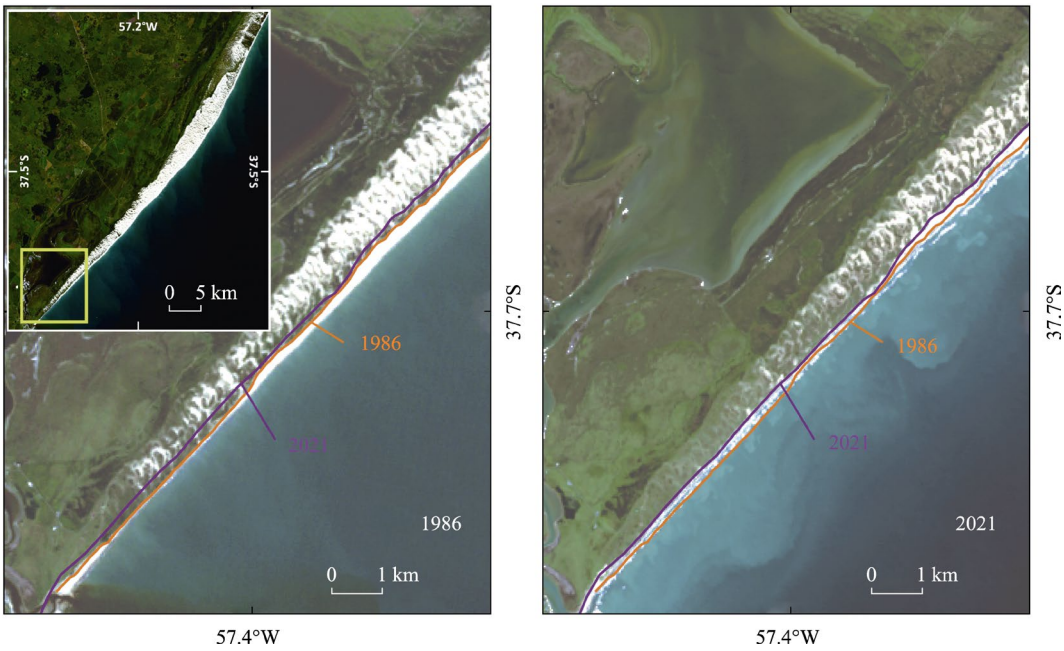

Figure 7 Comparison between 1986 (left) and 2021 (right) Landsat images for the southernmost sector of the study area. Color lines represent the location where vegetation establishment begins. Considered images: 01/06/1986 and 12/24/2021, respectively.

4.1 Drivers in vegetation cover changes (1986–2021)

The LCC change assessment and the NDVI time-series analysis revealed two main spatial patterns over the study period. Firstly, in the case of the northern villages (NV) and their surrounding private estates (PL-NV), the NDVI evolution was characterized by both periods of increase and decrease with differences among the vegetation classes between 1986 and 2021 (Figure 5).

The northern villages exhibited a cyclic pattern of expansion and contraction of urban vegetation, with minimum values for 1993 and 2011 and maximum values for 2000 and 2021 (Figure 8). These anthropogenic landscape modifications are linked to historical Argentine macroeconomic policies (Sala, 2021). Minimum urban coverage represents deforestation stages during periods of economic growth and touristic urbanization expansion, while the maximum afforestation stages are related to a lack of investment in the touristic sector.

In addition, the fluctuation in urban vegetation in the northern villages' zone was accompanied by an almost inversely proportional evolution in Pampean lowlands' vegetation and a gradual and irreversible decrease in herbaceous covers (Figure 8). These results indicate a two-stage successional mechanism for this zone: 1) afforestation promotes the replacement of dune areas or herbaceous dune vegetation by tree species; 2) deforestation creates space availability for Pampean lowlands' vegetation. This mechanism corresponds with evidence suggesting that changes in abiotic conditions (water resources, thermal range, soil environment, nutrient availability) triggered by dune afforestation initiatives can create favorable conditions for the establishment of immigrant species (Provoost *et al*., 2010). Moreover, the vertical structure of the anthropogenic canopies created by afforestation could facilitate the

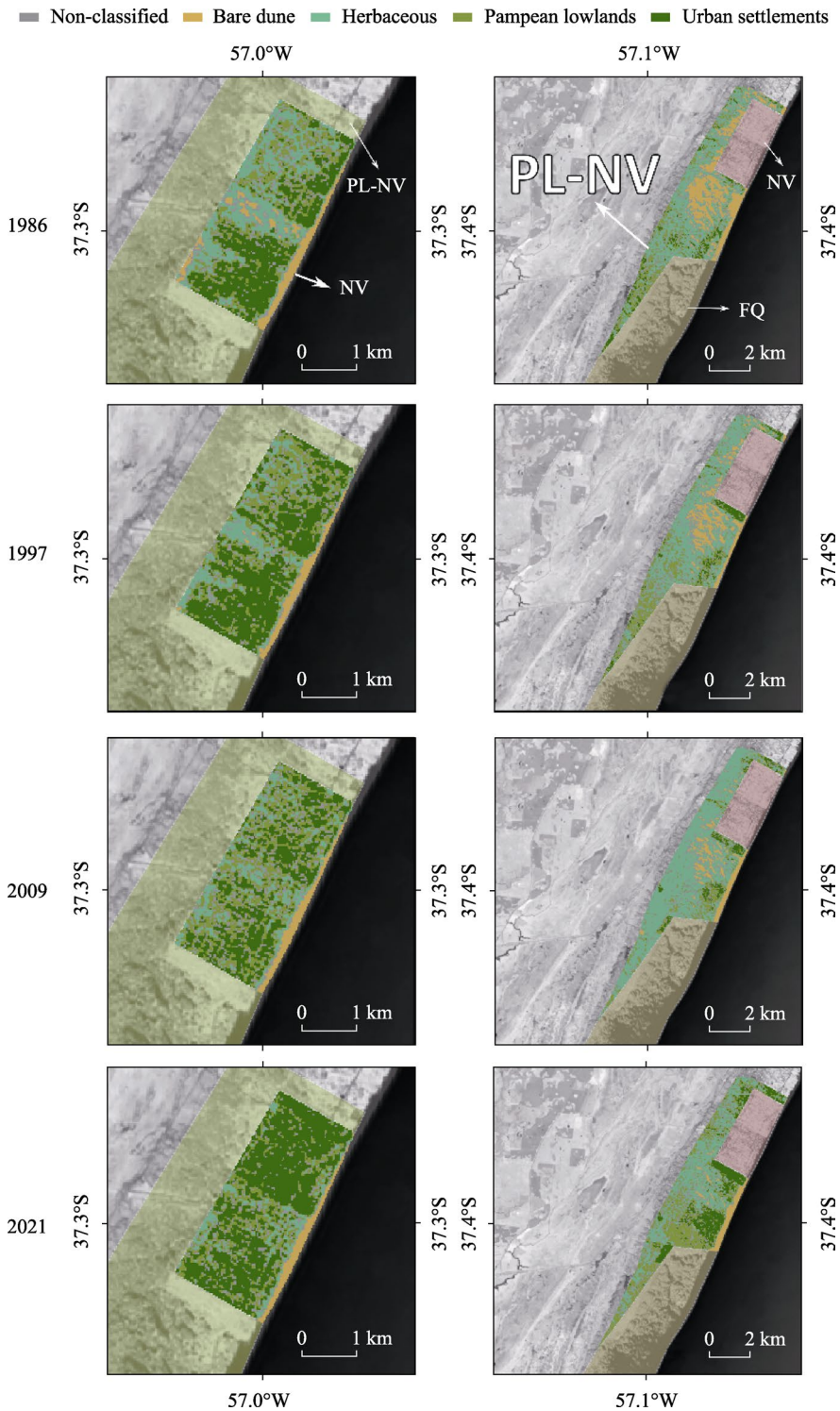

Figure 8 LCCs' spatial distribution in 1986, 1997, 2009, and 2021 for NV and PL-NV zones

unintentional introduction of other species, facilitating its dispersal by trapping wind-dispersed propagules. Faggi and Dadon (2011) have identified wind-blown seeds of *Lagurus ovatus,*

Dactylis glomerata, and *Festuca arundinacea* trapped in Villa Gesell woods, which are typical Pampean grasses in the surrounding rural areas.

The private estates (PL-NV) showed a similar pattern, with fluctuating urban coverage until 2015. Subsequently, a rapid increase was observed, reaching its greater surface in 2021. These results are directly linked to the development of country clubs and private neighborhoods. These new models of urban settlements were promoted by the Buenos Aires province in decrees No.9404/86 and 27/98, providing more incentives for private developers, comprising also coastal barriers. In the PL-NV zone, two of these developments ("Chacras del Mar" and "El Salvaje") were approved by the Villa Gesell County in 2015 under Ordinance No.2624, even when they still lack approval from the province's authorities. Consequently, the trend of dune-to-vegetation replacement in these zones appears to be irreversible, but its rate may be directly related to socio-economic factors.

The second spatial pattern was related to the vegetation coverage of the nature reserves. Given their conservation status, these zones have never been a priori directly subjected to anthropogenic drivers. Thus, climatic and geomorphological factors (variations in wind energy and aeolian transport, rainfall and humidity conditions, and sand supply driven by littoral drift) should be expected to explain the observed behavior.

The Faro Querandí and the Mar Chiquita reserves exhibited a gradual decrease in their dune area of ~50% and ~60%, respectively. The intra-reserves private estate (PL-IR) was consistent with this evolution, presenting a ~45% reduction in dune surface (Figure 9). For FQ and PL-IR zones, this pattern was accompanied by an inversely proportional expansion in herbaceous and Pampean covers and ~50% decreases in urban vegetation. The MC reserve, in contrast, presented gradual increases in herbaceous and Pampean vegetation, accompanied by a 70% increase in urban covers, mainly concentrated between 2011 and 2021.

Regarding the direction of vegetation changes, the FQ and PL-IR zones showed a gradual and constant pattern of herbaceous vegetation advance from W to E, mainly originating from pre-established nuclei. Accordingly, plant cover, diversity, and endemism showed patterns characterized by the increase from the distal beach landwards, reaching maximum values in the stable dunes (Calderisi *et al*., 2021). Pampean vegetation, in contrast, exhibited a gradual advance over urban vegetation, reaching an equilibrium scenario between 2000 and 2021. Almost the entire replacement of U vegetation was driven by P covers in the western boundaries of these zones. These original trees could be related to the establishment of vegetation fences of "Siempre Verde" *Myoporum laetum* (Marcomini *et al*., 2017). Once again, these patterns revealed that Pampean lowlands' vegetation exploits the ecological availability in a later successional stage related to the urban vegetation rollback.

In MC reserve, the gradual and consistent advance in herbaceous vegetation was observed following a bidirectional pattern: 1) from west to east, originating from pre-established nuclei; and 2) from east to west, in response to shoreline retreat and the landward shifting of dune pioneer species (Figure 7). Additionally, afforestation showed an ongoing increase in a W-E direction. This pattern is associated with the afforestation initiatives conducted in the neighboring private lands (Romano Estancia), which extended into the dune reserve areas. As with the other zones, these results indicate that the dynamics of U vegetation are closely related to anthropogenic activities (afforestation or deforestation stages). This suggests that stressful environmental conditions might act as a barrier to alien invasion (Sobrino *et al*.,

2002). These findings coincide with those obtained by Faggi and Dadon (2011), who pointed out that until 2006 there had been no danger of invasions by exotic fast-growing trees for this barrier system.

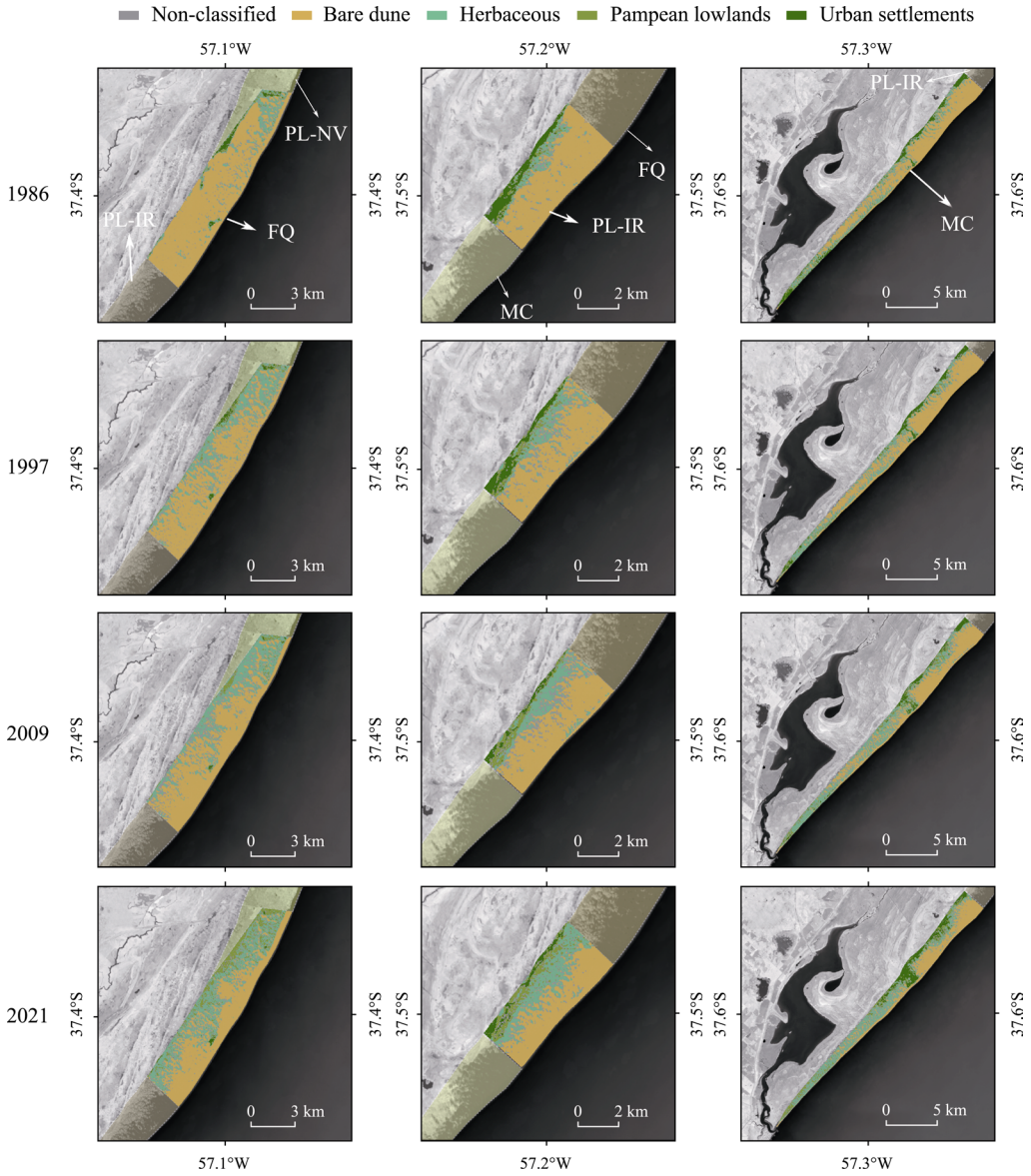

Figure 9 LCCs' spatial distribution in 1986, 1997, 2009, and 2021 for FQ, PL-IR, and MC zones

4.2 Are regional sand savings at risk?

More than 80% of the world's coastal barriers are currently impacted by anthropic activities (Gao *et al*., 2020). Provoost *et al*. (2011) have documented an extensive dune fixation process across most coastal dunes in Western Europe. Consequently, the influence of LULC changes on dune mobility is an ongoing global concern, further exacerbated by the effects of

climate change. In arid and semi-arid dune regions, the increase in drought conditions is leading to greater dune mobility (Thomas *et al*., 2005). However, patterns of increased rainfall are promoting, by natural- or anthropic-induced processes, the greening and the subsequent reduced mobility of coastal dunes on a global scale (Jackson *et al*., 2019). The results of this study are consistent with a gradual and irreversible greening of the dune fields of the Eastern Sandy Barrier. In addition, greening would increase according to the IPCC's rainfall forecast for the SE areas of South America (Magrin *et al*., 2014). At the same time, the bias induced by the effects of strong ENSOs would signify a greater inter- and intra-annual variability as recorded in previous periods (1997–1998).

The dune mobility reduction is directly linked to sediment imbalances in beach-dune systems and coastal erosion in barrier sectors (Illenberger, 1993). The reduced mobility can result in foredune growth at the expense of a reduction in beach areas (Kratzmann and Hapke 2012). As a consequence, shoreline retreat can cause several socioeconomic impacts, in particular those related to a loss in the recreational and touristic value of beaches (Mentaschi *et al*., 2018).

A total replacement of 4245 ha of bare dunes by vegetation was assessed, with 3250 ha falling within the boundaries of nature reserves. The dune/vegetation ratio decreased from 1.75 to 0.42 between 1986 and 2021. Within the nature reserves, this ratio was even more critical, ranging from 2.14 to 0.39 during the same period. This dune-to-vegetation replacement was driven by an expansion of 2242 ha of herbaceous vegetation, 1498 ha of Pampean lowland vegetation, and 505 ha of forestry and gardening vegetation. More than 65% of the plant expansion in the reserves can be attributed to herbaceous covers.

The LULC impacts can be traced to the local geomorphological dynamics. Shoreline retreat trends of 0.24 m/yr between 1965 and 2021 were documented for the northern villages' zone, attributed to the cross-shore sedimentary imbalances induced by afforestation initiatives over urban areas (Garzo *et al*., 2023). The Faro Querandí and Mar Chiquita nature reserves currently comprise more than 10% of the Eastern Sandy Barrier's surface and represent the only remaining environments with low local anthropic impacts in the region (Celsi, *et al*., 2016). Given this context, their greening and the subsequent reduction in these extensive "sand savings" could potentially disrupt one of their primary objectives: the preservation of the regional sedimentary balance. Future research must address this issue, aiming to evaluate geomorphological constraints and sedimentary imbalances resulting from vegetation expansion through high-temporal-sustainable field surveys and high-resolution geospatial analysis.

4.3 Dune management facing a forecasted greening

The ANN approach, powered by the MOLUSCE tool, showed an overall accuracy consistent with previous studies on vegetation covers (Kafy *et al*., 2021). For FQ and PL-IR zones, the projected scenario for 2050 indicates a gradual reduction in dune areas, with a corresponding expansion of herbaceous and Pampean vegetation. This scenario replicates the 1986–2021 results, which indicated a west-to-east vegetation advance, primarily originated from pre-established plant nuclei. The changes would lead to a dune/vegetation ratio of 0.34 for both zones, restricting bare sand to approximately 30% of their total surface, mainly located in the beach section of the barrier. In the zones with a low degree of human intervention, the

forecasted behavior can be attributed to climatic and geomorphological factors, which were also associated with the 1986–2021 observed changes.

In contrast, for NC, PL-NV, and MC zones, the predicted scenario indicates negligible reductions in dune areas and a systematic replacement of herbaceous or Pampean lowland's vegetation by afforestation and gardening species. At this point, the projected changes could be directly linked to the anthropogenic influence over the contraction and retraction periods of afforestation initiatives and touristic urban development, which reduces the reliability of the forecasted scenarios.

The Villa Gesell County has recently approved an Urbanization Plan (Plan de Ordenamiento Municipal; Ordinance No.3138/21). It projects a shift in the tourism development of the northern villages, with a projected increase in population of 65.000 inhabitants by 2044. In addition, a new urban development spanning 1,260 ha is planned for their surrounding private lands. The urban area will cover a 4-km linear shoreline extension with a potential population of 35.000 inhabitants.

According to Decree No.8912/77, the development of new urban areas in the dune fields of Buenos Aires province requires prior stabilization and afforestation of the dunes. Moreover, the urbanization density must allow for the sustainability of these afforestation initiatives. Since dune stabilization actions will be imperative in Villa Gesell, the urbanization plan establishes dune fixation using low water-consumption herbaceous species and trees lower than 15 m-height. Thus, the introduction of exotic species or even afforestation by fast-growing exotic trees is not explicitly banned. This approach refutes previous studies for the zone, which recommend the use of native species for new dune fixation areas, aiming to restore the original dune landscape (Isla *et al*., 2022). Based on these future greening scenarios, proper management of the beach-dune system is strictly necessary for the maintenance of the local, and even regional, sediment balance. At this point, some considerations must be taken into account.

In those areas subjected to afforestation initiatives in the past, deforestation has been recognized as a useful strategy for coastal dune restoration (Litghow *et al*., 2013). However, dune deforestation is prohibited in the Buenos Aires province according to the aforementioned Decree No.8912/77. In addition, despite their documented environmental impacts, coastal forests are considered an invaluable community heritage, being part of the local cultural identity. For these reasons, a generalized deforestation strategy does not appear as a viable option, but the avoidance of new afforestation initiatives with exotic trees must be ensured. The management of dune areas that will be imperatively fixed must ensure the exclusive establishment of herbaceous native species. This may pose a challenge for stakeholders and managers, as the current paradigm suggests that native species have no potential for fixation.

According to the results of this study, the rate of afforestation and deforestation initiatives is directly related to socio-economic factors. Beyond this, there is no danger of invasions by exotic fast-growing trees. However, the invasiveness of Pampean lowlands' vegetation, by exploiting the ecological availability in deforestation stages, has been demonstrated. Invasive species pose a significant threat to native species worldwide (Vitousek *et al*., 1997). Management actions must focus on removing invasive species and aim to restore native dune vegetation communities in urban areas as well as in nature reserves. Nevertheless, in-

vasive species might set several challenges when attempting to re-introduce native species in coastal dune environments (Novoa *et al*., 2013). The restoration of native species requires a long-term approach by guaranteeing the reduction of the density of invader species and the sowing of native seeds and/or planting of established seedlings (Vranjic *et al*., 2012). This process could be supported by physical substrate stabilization using sand fences (Van der Meulen and Salman, 1996). The success of this restoration will depend on the capacity of native species to recolonize the area and compete for available resources with the managed invader species (Mason, 2007).

5 Conclusions

This paper presents a large-scale vegetation assessment for the Eastern Sandy Barrier of Buenos Aires, Argentina. The evaluation relied on the spectral analysis of an extensive satellite database processed using Google Earth Engine, marking the first application of this platform for this coastal region. Beyond the overall performance of the study, its limitations were related to the surface heterogeneity, the spatial resolution of satellite imagery, and the influence of ENSO periods and climate variability. Moreover, afforestation projects and touristic urban development reduce the reliability of the results obtained for the 2050 forecast in some areas.

The study area exhibited a smoothly progressive trend of vegetation expansion between 1986 and 2021, characterized by the replacement of more than 4,200 ha of dune areas with green covers. In 1986, the dune area comprised 75% more surface than vegetation, whereas in 2021, it represented 60% less than vegetation. The Faro Querandí and Mar Chiquita nature reserves faced an even more critical situation, with their dune areas reduced by more than half, mainly driven by a gradual and consistent advance of herbaceous vegetation in a west-east direction. In addition, the predicted scenario for 2050 indicates a gradual reduction in dune areas of the Faro Querandí reserve, restricting the bare sand to only 30% of its total surface. Despite this, the dynamics of exotic urban vegetation suggest that afforestation does not pose a danger of spontaneous invasion over dune areas. In contrast, coastal resorts and private estates exhibited a cyclic pattern characterized by anthropogenic-driven expansion and contraction of urban vegetation, with a. rapid increase in afforestation practices concurrent with the development of private neighborhoods since 2015. This fluctuating pattern was accompanied by an inversely proportional evolution in Pampean vegetation, suggesting that changes in abiotic conditions triggered by afforestation can promote favorable conditions for immigrant and invasive species. Consequently, the trend of dune-to-vegetation replacement was irreversible, but its rate may be directly linked to anthropogenic activities and socio-economic factors.

The Villa Gesell County has recently approved an urbanization plan that includes dune fixation initiatives. In consequence, the historical evolution of vegetation covers, as well as projected future scenarios or even current urbanization plans, point towards a generalized greening. Moreover, the effects of climate change are expected to exacerbate this scenario. These processes will inexorably promote a reduction in dune mobility, altering the sedimentary balance, promoting coastal erosion, and causing several socioeconomic impacts. Therefore, it is important to enhance proper management strategies aimed at maintaining the local

and regional sediment balance. It is suggested that future dune fixation initiatives adopt a native-species approach. This represents a major challenge for managers, as it involves cultural, regulatory, and social constraints. It is expected that the results of this study will be useful for urban beaches as well as nature reserve management.

Abbreviations

ANN = Artificial Neural Network; D = Bare dune areas; FQ = Faro Querandí Nature Reserve; GEE = Google Earth Engine; H = Herbaceous dune vegetation; LCC = Land cover class; MC = Mar Chiquita Nature Reserve; NV = Northern villages; P = Pampean lowlands' vegetation; PL-IR = Intra-reserves' private lands; PL-NV = Northern villages' private lands; U = Urban settlements' vegetation.

Funding

This work was supported by the Ministry of Science, Technology and Innovation of Argentina trough the project "Topografía, escurrimiento superficial y monitoreo de playas en el Partido de Villa Gesell, provincia de Buenos Aires" (Impact.AR N°106 - RESOL-2022-224-APN-SACT#MCT); and by the Nacional Council of Scientific and Technical Research (CONICET) through the project "Impactos de la reversión del nivel del mar en Buenos Aires, Argentina" (PIP 21/23 11220200100041CO - RESOL-2021-1639-APN-DIR#CONICET).

Authors' contributions

P.A. Garzo: Investigation, Methodology, Software, Formal Analysis, Data Curation; Visualization, Writing – Original Draft, Writing – Review & Editing. J.R. Dadon: Conceptualization, Investigation, Supervision, Methodology, Writing – Original Draft, Writing – Review & Editing. F.I. Isla: Writing – Original Draft, Writing – Review & Editing, Funding Acquisition. All authors read and approved the final manuscript.

Declaration of competing interest

The authors declare that they have no known competing financial interests or personal relationships that could have appeared to influence the work reported in this paper.

Acknowledgements

The authors acknowledge the Environmental Department of Villa Gesell County, in particular Lic. M. Gore-Parravicini, for supporting our work.

References

Anthonsen K L, Clemmensen L B, Jensen J H, 1996. Evolution of a dune from crescentic to parabolic form in response to short-term climatic changes: Råbjerg Mile, Skagen Odde, Denmark. *Geomorphology*, 17(1–3): 63–77. https://doi.org/10.1016/0169-555x(95)00091-i.

Avis A M, 1989. A review of coastal dune stabilization in the Cape Province of South Africa. *Landscape and Urban Planning*, 18(1): 55–68. https://doi.org/10.1016/0169-2046(89)90055-8.

Baeza S, Paruelo J M, 2020. Land use/land cover change (2000–2014) in the Rio de la Plata grasslands: An analysis based on MODIS NDVI time series. *Remote Sensing*, 12(3): 381. https://doi.org/10.3390/rs1203038 1.

Busayo E T, Kalumba A M, 2021. Recommendations for linking climate change adaptation and disaster risk reduction in urban coastal zones: Lessons from East London, South Africa. Ocean & Coastal Management, 203: 105454. https://doi.org/10.1016/j.ocecoaman.2020.105454.

Bustos M L, Ferrelli F, Piccolo M C, 2016. El rol del arbolado urbano sobre la temperatura invernal de la villa balnearia de Pehuen Co (Argentina). *Revista Universitaria de Geografía*, 25(1): 57–72.

Cabrera A L, 1941. Las comunidades vegetales de las dunas costaneras de la provincia de Buenos Aires. DAGI, 1(2): 1–44.

Calderisi G, Cogoni D, Pinna M S *et al*., 2021. Recognizing the relative effects of environmental versus human factors to understand the conservation of coastal dunes areas. *Regional Studies in Marine Science*, 48: 102070. https://doi.org/10.1016/j.rsma.2021.102070.

Castillo S A, Moreno-Casasola P, 1996. Coastal sand dune vegetation: An extreme case of species invasion. *Journal of Coastal Conservation*, 2(1): 13–22. https://doi.org/10.1007/bf02743033.

Celsi C E, 2016. La vegetación de las dunas costeras pampeanas. La Costa Atlántica de Buenos Aires. Naturaleza y Patrimonio Cultural. Fundación de Historia Natural Félix de Azara, 116–138.

Celsi C E, Cenizo M, Sotelo M *et al*., 2016. Las áreas naturales protegidas de la costa bonaerense. In: La Costa Atlántica de Buenos Aires. Naturaleza y Patrimonio Cultural, Fundación de Historia Natural Félix de Azara, 487–527.

Chen D, Wang Y, Shen Z *et al*., 2021. Long time-series mapping and change detection of coastal zone land use based on Google Earth engine and multi-source data fusion. *Remote Sensing*, 14(1): 1. https://doi.org/10.3390/rs14010001.

Clark J R, 1997. Coastal zone management for the new century. *Ocean & Coastal Management*, 37(2): 191–216. https://doi.org/10.1016/s0964-5691(97)00052-5.

Congedo L, 2021. Semi-Automatic Classification Plugin: A Python tool for the download and processing of remote sensing images in QGIS. *Journal of Open Source Software*, 6(64): 3172. https://doi.org/10.21105/joss.03172.

Cortizo L C, Isla F I, 2012. Dinámica de la barrera medanosa e islas de barrera de Patagones (Buenos Aires, Argentina). *Latin American Journal of Sedimentology and Basin Analysis*, 19(1): 47–63.

Da Silva D D P, Schwingel P R, 2019. Influência do turismo como fator estressor na evolução do uso e ocupação do solo em municípios da costa de Santa Catarina. *Journal of Integrated Coastal Zone Management*, 19(1): 17–25. https://doi.org/10.5894/rgci-n195.

Defra, 2007. Management for flood and coastal defense (Part 4): Techniques for sand dune management. Department for Environment, Food & Rural Affairs, UK. R&D Technical Report FD1302/TR London, 49pp.

Di Rienzo J A, Casanoves F, Balzarini M G *et al*., 2020. InfoStat versión 2020. Centro de Transferencia InfoStat, FCA, Universidad Nacional de Córdoba, Argentina. URL http://www.infostat.com.ar.

Doody J P, 2005. Shoreline management: Conservation, management or restoration. In: Herrier J-L, Mees J, Salman A *et al*. (eds). Proceedings 'Dunes and Estuaries', 407–419.

Doughty C L, Ambrose R F, Okin G S *et al*., 2021. Characterizing spatial variability in coastal wetland biomass across multiple scales using UAV and satellite imagery. *Remote Sensing in Ecology and Conservation*, 7(3): 411–429. https://doi.org/10.1002/rse2.198.

Faggi A M, Dadon J R, 2010. Vegetation changes associated to coastal tourist urbanizations. *Multequina*, 19: 53–76.

Faggi A M, Dadon J R, 2011. Temporal and spatial changes in plant dune diversity in urban resorts. *Journal of Coastal Conservation*, 15: 585–594. https://doi.org/10.1007/s11852-011-0148-1.

Fairbanks D H, Mcgwire K C, 2004. Patterns of floristic richness in vegetation communities of California: Regional scale analysis with multi-temporal NDVI. *Global Ecology and Biogeography*, 13(3): 221–235. https://doi.org/10.1111/j.1466-822x.2004.00092.x.

Feagin R A, Mukherjee N, Shanker K *et al*., 2010. Shelter from the storm? Use and misuse of coastal vegetation bioshields for managing natural disasters. *Conservation Letters*, 3(1): 1–11. https://doi.org/10.1111/j.1755-263x.2009.00087.x.

Fitton J M, Rennie A F, Hansom J D, *et al*., 2021. Remotely sensed mapping of the intertidal zone: A Sentinel-2 and Google Earth Engine methodology. *Remote Sensing Applications*: *Society and Environmen*t, 22, 100499. https://doi.org/10.1016/j.rsase.2021.100499.

Framiñan M, 1990. Transporte de sedimentos en Pinamar, Provincia de Buenos Aires. II Jornadas de Oceanografía

Física y XVI Reunión Científica de la Asociación Argentina de Geofísicos y Geodestas: 15. Bahía Blanca, Argentina.

Gao J, Kennedy D M, Konlechner T M, 2020. Coastal dune mobility over the past century: A global review. *Progress in Physical Geography*: *Earth and Environment*, 44(6): 814–836. https://doi.org/10.1177/0309133320919612.

Garzo P A, Dadon J R, Castro L N, 2019. Modeling environmental vulnerability of the Biosphere Reserve Parque Atlántico Mar Chiquito, Argentina, under agricultural and urban impacts. *Ocean & Coastal Management*, 170: 72–79. https://doi.org/10.1016/j.ocecoaman.2019.01.004.

Garzo P A, Sánchez-Caro L, Mojica M, 2023. Coastal erosion in temperate barriers: An anthropized sandy beach in Buenos Aires, Argentina. *Journal of South American Earth Sciences*, 104453. https://doi.org/10.1016/j.jsames.2023.104453.

Ghebrezgabher M G, Yang T, Yang X *et al*., 2020. Assessment of NDVI variations in responses to climate change in the Horn of Africa. *The Egyptian Journal of Remote Sensing and Space Science*, 23(3): 249–261. https://doi.org/10.1016/j.ejrs.2020.08.003.

González Trilla G, Pratolongo P, Beget M E *et al*., 2013. Relating biophysical parameters of coastal marshes to hyperspectral reflectance data in the Bahia Blanca Estuary, Argentina. *Journal of Coastal Research*, 29(1): 231–238. https://doi.org/10.2112/jcoastres-d-11-00214.1.

González Trilla G, Pratolongo P, Kandus P *et al*., 2016. Relationship between biophysical parameters and synthetic indices derived from hyperspectral field data in a salt marsh from Buenos Aires Province, Argentina. *Wetlands*, 36: 185–194. https://doi.org/10.1007/s13157-015-0715-6.

Goñi L, Gregorini G, Aldalur B, 2016. Análisis del crecimiento edilicio mediante imágenes Landsat en la localidad de Monte Hermoso, Argentina. Actas del 2° Encuentro Nacional de Investigadores de Agrimensura. Santa Fe, Argentina, 1–8.

Gómez-Pina G, Muñoz-Pérez J J, Ramírez J L *et al*., 2002. Sand dune management problems and techniques, Spain. *Journal of Coastal Research*, 36: 325–332. https://doi.org/10.2112/1551-5036-36.sp1.325.

Gorelick N, Hancher M, Dixon M *et al*., 2017. Google Earth Engine: Planetary-scale geospatial analysis for everyone. *Remote Sensing of Environment*, 202: 18–27. https://doi.org/10.1016/j.rse.2017.06.031.

Gu J, Li X, Huang C *et al*., 2009. A simplified data assimilation method for reconstructing time-series MODIS NDVI data. *Advances in Space Research*, 44(4): 501–509. https://doi.org/10.1016/j.rse.2017.06.031.

Hesp P, Schmutz P, Martinez M M *et al*., 2010. The effect on coastal vegetation of trampling on a parabolic dune. *Aeolian Research*, 2(2/3): 105–111. https://doi.org/10.1016/j.aeolia.2010.03.001.

Huang J, Wang H, Dai Q *et al*., 2014. Analysis of NDVI data for crop identification and yield estimation. *IEEE Journal of Selected Topics in Applied Earth Observations and Remote Sensing*, 7(11): 4374–4384. https://doi.org/10.1109/jstars.2014.2334332.

Illenberger W K, 1993. Variations of sediment dynamics in Algoa Bay during the Holocene. *South African Journal of Science*, 89(4): 187–196.

Isla F I, 1998. Holocene coastal evolution in Buenos Aires province, Argentina. In: Quaternary of South America and Antarctic Peninsula. Routledge, 297–321. https://doi.org/10.1201/9780203741429-17.

Isla F I, 2013. From touristic villages to coastal cities: The costs of the big step in Buenos Aires. *Ocean & Coastal Management*, 77: 59–65. https://doi.org/10.1016/j.ocecoaman.2012.02.005.

Isla F I, Bértola G R, Farenga M O *et al*., 1998. Villa Gesell: Un desequilibrio sedimentario inducido por fijaciones de médanos. *Revista de la Asociación Argentina de Sedimentología*, 5(1): 41–51.

Isla F I, Garzo P A, Sánchez-Caro L, 2022. Environmental evolution of coastal afforestations: Management strategies for dune fixation in the sandy barriers of Buenos Aires, Argentina. *Journal of Integrated Coastal Zone Management*, 22(3): 207–224. https://doi.org/10.5894/rgci-n516.

Jackson D W, Costas S, González-Villanueva R *et al*., 2019. A global 'greening' of coastal dunes: An integrated consequence of climate change? *Global and Planetary Change*, 182: 103026. https://doi.org/10.1016/j.gloplacha.2019.103026.

Juárez V, Isla F, 1999. Evolución histórica del núcleo urbano de Villa Gesell. *Revista Geográfica*, 49–60.

Kafy A A, Dey N N, Al Rakib A *et al*., 2021. Modeling the relationship between land use/land cover and land surface temperature in Dhaka, Bangladesh using CA-ANN algorithm. *Environmental Challenges*, 4: 100190. https://doi.org/10.1016/j.gloplacha.2019.103026.

Klein Y L, Osleeb J, 2010. Determinants of coastal tourism: A case study of Florida beach counties. *Journal of Coastal Research*, 26(6): 1149–1156. https://doi.org/10.2112/jcoastres-d-09-00152.1.

Kratzmann M G, Hapke C J, 2012. Quantifying anthropogenically driven morphologic changes on a barrier island: Fire Island National Seashore, New York. *Journal of Coastal Research*, 28(1): 76–88. https://doi.org/10.2112/jcoastres-d-10-00012.1.

Lanfredi N W, Pousa J L, Mazio C A *et al*., 1992. Wave-power potential along the coast of the province of Buenos Aires, Argentina. *Energy*, 17(11): 997–1006. https://doi.org/10.1016/0360-5442(92)90016-s.

Li W, Liu C, Hong Y *et al*., 2016. Rainstorm-induced shallow landslides process and evaluation: A case study from three hot spots, China. *Geomatics*, *Natural Hazards and Risk*, 7(6): 1908–1918. https://doi.org/10.1080/19475705.2016.1179685.

Lithgow D, Martínez M L, Gallego-Fernández J B *et al*., 2013. Linking restoration ecology with coastal dune restoration. *Geomorphology*, 199: 214–224. https://doi.org/10.1016/j.geomorph.2013.05.007.

Luo S, Cai F, Liu H *et al*., 2015. Adaptive measures adopted for risk reduction of coastal erosion in the People's Republic of China. *Ocean & Coastal Management*, 103: 134–145. https://doi.org/10.1016/j.ocecoaman.2014.08.008.

Magrin G O, Marengo J A, Boulanger J P *et al*., 2014. Central and South America. In: Climate Change 2014: Impacts, Adaptation, and Vulnerability. Part B: Regional Aspects. Contribution of Working Group II to the Fifth Assessment Report of the Intergovernmental Panel on Climate Change Cambridge University Press, Cambridge, United Kingdom and New York, NY, USA, 1499–1566. https://doi.org/10.1017/cbo9781107415386.007.

Marcomini S, López R, Picca P *et al*., 2017. Natural coastal dune-field landforms, plant communities, and human intervention along Buenos Aires Northern Aeolian Barrier. *Journal of Coastal Research*, 33(5): 1051–1064. https://doi.org/10.2112/jcoastres-d-15-00219.1.

Mason T J, French K, Russell K G, 2007. Moderate impacts of plant invasion and management regimes in coastal hind dune seed banks. *Biological Conservation*, 134(3): 428–439. https://doi.org/10.1016/j.biocon.2006.08.032.

Mentaschi L, Vousdoukas M I, Pekel J F *et al*., 2018. Global long-term observations of coastal erosion and accretion. *Scientific Reports*, 8(1): 12876. https://doi.org/10.1038/s41598-018-30904-w.

Muhammad R, Zhang W, Abbas Z *et al*., 2022. Spatiotemporal change analysis and prediction of future land use and land cover changes using QGIS MOLUSCE plugin and remote sensing big data: A case study of Linyi, China. *Land*, 11(3): 419. https://doi.org/10.3390/land11030419.

Muhs D R, Maat P B, 1993. The potential response of eolian sands to greenhouse warming and precipitation reduction on the Great Plains of the USA. *Journal of Arid Environments*, 25(4): 351–361. https://doi.org/10.1006/jare.1993.1068.

Novoa A, González L, Moravcová L *et al*., 2013. Constraints to native plant species establishment in coastal dune communities invaded by Carpobrotus edulis: Implications for restoration. *Biological Conservation*, 164: 1–9. https://doi.org/10.1016/j.biocon.2013.04.008.

Okello C, Antonellini M, Greggio N *et al*., 2015. Freshwater resource characterization and vulnerability to climate change of the Shela aquifer in Lamu, Kenya. *Environmental Earth Sciences*, 73: 3801–3817. https://doi.org/10.1007/s12665-014-3665-z.

Palma M, Dias J A, Freitas J G D, 2021. It's not only the sea: A history of human intervention in the beach-dune ecosystem of Costa da Caparica (Portugal). *Journal of Integrated Coastal Zone Management*, 21: 227–247. https://doi.org/10.5894/rgci-n432.

Paruelo J M, Garbulsky M F, Guerschman J P *et al*., 2004. Two decades of Normalized Difference Vegetation Index changes in South America: identifying the imprint of global change. *International Journal of Remote Sensing*, 25(14): 2793–2806. https://doi.org/10.1080/01431160310001619526.

Pauchard A, Aguayo M, Peña E *et al*., 2006. Multiple effects of urbanization on the biodiversity of developing countries: The case of a fast-growing metropolitan area (Concepción, Chile). *Biological Conservation*, 127(3): 272–281. https://doi.org/10.1016/j.biocon.2005.05.015.

Pilkey O H, Cooper A G, Lewis D A, 2009. Global distribution and geomorphology of fetch-limited barrier islands. *Journal of Coastal Research*, 25: 819–837. https://doi.org/10.2112/08-1023.1.

Pintó J, García-Lozano C, Varga D, 2023. Using dune-restricted species to assess the degree of natural diversity of dune systems on Mediterranean tourist coasts. *Ecological Indicators*, 147: 110004. https://doi.org/10.1016/j.ecolind.2023.110004.

Pranzini E, 2018. Coastal erosion and shore protection: A brief historical analysis. *Journal of Coastal Conservation*, 22(5): 827–830. https://doi.org/10.1007/s11852-017-0521-9.

Provoost S, Jones M L M, Edmondson S E, 2011. Changes in landscape and vegetation of coastal dunes in northwest Europe: A review. *Journal of Coastal Conservation*, 15: 207–226. https://doi.org/10.1007/s11852-009-0068-5.

Python Software Foundation, 2023. Python Language Reference, version 3.11.3. Available at: https://docs. python.org/3/reference/.

Qgis Development Team, 2022. QGIS Geographic Information System. Open-Source Geospatial Foundation Project. Available at: http://qgis.osgeo.org.

Ratas U, Rivis R, Käärt K, 2008. Changes of coastal dune landscapes in Estonia. *Forestry Studies*, 49(2008): 59–70. https://doi.org/10.2478/v10132-011-0063-0.

Roy D P, Kovalskyy V, Zhang H K *et al*., 2016. Characterization of Landsat-7 to Landsat-8 reflective wavelength and normalized difference vegetation index continuity. *Remote Sensing of Environment*, 185: 57–70. https://doi.org/10.1016/j.rse.2015.12.024.

Sala M E, 2021. Turismo internacional y ciclos económicos: ¿Es el turismo un sector estratégico para superar los tiempos recesivos? Estudio de caso Argentina 1990–2015. Licentiate Thesis. Universidad Abierta Interamericana, Argentina, 121 pp. Available at: https://repositorio.uai.edu.ar/handle/123456789/93.

Schlacher T A, Schoeman D S, Dugan *et al*., 2008. Sandy beach ecosystems: key features, sampling issues, management challenges and climate change impacts. *Marine Ecology*, 29: 70–90. https://doi.org/10.1111/j.1439-0485.2007.00204.x.

Sobrino E, Sanz-Elorza M, Dana E D *et al*., 2002. Invasibility of a coastal strip in NE Spain by alien plants. *Journal of Vegetation Science*, 13(4), 585–594. https://doi.org/10.1111/j.1654-1103.2002.tb02085.x.

Stoms D M, Davis F W, Andelman S J *et al*., 2005. Integrated coastal reserve planning: making the land–sea connection. *Frontiers in Ecology and the Environment*, 3(8): 429–436. https://doi.org/10.1890/1540-9295(2005)003[0429:icrpmt]2.0.co;2.

Texeira-Pinto L H, Reis-Fernandes L, 2011. Multitemporal analyses of the vegetation cover of coastal sand dune ecosystems in Natal/RN, based on NDVI index. XV Simpósio Brasileiro de Sensoriamento Remoto. INPE, Curitiba, PR, Brasil, 1895–1901.

Thomas D S, Knight M, Wiggs G F, 2005. Remobilization of southern African desert dune systems by twenty-first century global warming. *Nature*, 435(7046): 1218–1221. https://doi.org/10.1038/nature03717.

Thomas V A, Wynne R H, Kauffman J *et al*., 2021. Mapping thins to identify active forest management in southern pine plantations using Landsat time series stacks. *Remote Sensing of Environment*, 252: 112127. https://doi.org/10.1038/nature03717.

Trepekli A, Loupa G, Rapsomanikis S, 2016. Seasonal evapotranspiration, energy fluxes and turbulence variance characteristics of a Mediterranean coastal grassland. *Agricultural and Forest Meteorology*, 226: 13–27. https://doi.org/10.1016/j.agrformet.2016.05.006.

Van Der Meulen F, Salman A H P M, 1996. Management of Mediterranean coastal dunes. *Ocean & Coastal Management*, 30(2/3): 177–195. https://doi.org/10.1016/0964-5691(95)00060-7.

Vijay R, Dey J, Sakhre S *et al*., 2020. Impact of urbanization on creeks of Mumbai, India: A geospatial assessment approach. *Journal of Coastal Conservation*, 24: 1–16. https://doi.org/10.1007/s11852-019-00721-y.

Vitousek P M, D'antonio C M, Loope L L *et al*., 1997. Introduced species: A significant component of human-caused global change. *New Zealand Journal of Ecology*, 1–16. https://doi.org/10.1016/0169-5347(87)90026-7.

Vranjic J A, Morin L, Reid A M *et al*., 2012. Integrating revegetation with management methods to rehabilitate coastal vegetation invaded by Bitou bush (Chrysanthemoides monilifera ssp. rotundata) in Australia. *Austral Ecology*, 37(1): 78–89. https://doi.org/10.1111/j.1442-9993.2011.02242.x.

Wang Q, Adiku S, Tenhunen J *et al*., 2005. On the relationship of NDVI with leaf area index in a deciduous forest site. *Remote Sensing of Environment*, 94(2): 244–255. https://doi.org/10.1016/j.rse.2004.10.006.

Weiss J L, Gutzler D S, Coonrod J E A *et al*., 2004. Long-term vegetation monitoring with NDVI in a diverse semi-arid setting, central New Mexico, USA. *Journal of Arid Environments*, 58(2): 249–272. https://doi.org/10.1016/j.jaridenv.2003.07.001.

Zhao Q, Pan J, Devlin A T, 2022. On the exploitation of remote sensing technologies for the monitoring of coastal and river delta regions. *Remote Sensing*, 14(10): 2384. https://doi.org/10.3390/rs14102384.